Impact of human activities and vegetation changes on the tetraether sources in Lake St Front (Massif Central, France)

Céline Martin, Guillemette Ménot, Nicolas Thouveny, Nina Davtian, Valérie Andrieu-Ponel, Maurice Reille, Edouard Bard

Impact of human activities and vegetation changes on the tetraether sources in Lake St Front (Massif Central, France)

Céline Martin, Guillemette Ménot, Nicolas Thouveny, Nina Davtian, Valérie Andrieu-Ponel, Maurice Reille, Edouard Bard

PII: S0146-6380(19)30106-8
DOI: https://doi.org/10.1016/j.orggeochem.2019.06.005
Reference: OG 3884

To appear in: *Organic Geochemistry*

Received Date: 18 February 2019
Revised Date: 12 June 2019
Accepted Date: 13 June 2019

Impact of human activities and vegetation changes on the tetraether sources in Lake St Front (Massif Central, France)

Céline Martin[a,b]*, Guillemette Ménot[b], Nicolas Thouveny[a], Nina Davtian[a], Valérie Andrieu-Ponel[c], Maurice Reille[d], Edouard Bard[a]

[a] *Aix Marseille Univ, CNRS, IRD, INRA, Coll France, CEREGE, Europôle Méditerranéen de l'Arbois BP 80 13545 Aix-en-Provence Cedex 4, France*

[b] *Université de Lyon, ENSL, UCBL, CNRS, LGL-TPE, 46 allée d'Italie, 69364 Lyon Cedex 7, France*

[c] *Aix Marseille Univ, Univ Avignon, CNRS, IRD, IMBE, Europôle Méditerranéen de l'Arbois BP 80 13545 Aix-en-Provence Cedex 4, France*

[d] *Venède, 48000 Mende, France*

*Corresponding author: Céline Martin, LGL-TPE, Ecole Normale Supérieure de Lyon, 46 Allée d'Italie, 69364 Lyon Cedex 7, France. E-mail: celine.martin@ens-lyon.fr, tel: +33 6 20 75 60 91

ABSTRACT

The distribution of branched glycerol dialkyl glycerol tetraethers (brGDGTs) has been shown to correlate with mean annual air temperature and is increasingly used for paleoclimate reconstructions, in particular in lakes. Numerous studies have reported in situ production of brGDGTs in lakes. These brGDGTs have different distributions compared with those produced in soils and their mixing hampers paleoclimate reconstructions. Very few tools exist to determine brGDGT sources in the present and to trace their changes in the past linked with environmental changes of climatic or anthropogenic origin. While human activities are known to affect both soil and aquatic ecosystems, particularly bacterial communities, the specific impacts on brGDGT distributions are poorly investigated. High resolution analyses of brGDGTs were carried out on Holocene sediments and catchment soils of Lake St Front (Massif Central, France) in association with sedimentological, palynological, and geochemical analyses. Comparison of brGDGT distributions in sediments and soils revealed their mixed origin. For the first time, we tested the reliability of the ΣIIIa/ΣIIa ratio in lakes which indicated a gradual shift from aquatic to terrigenous brGDGT sources over the Holocene. This shift was supported by sedimentological and geochemical indices. Three events with a high proportion of terrigenous brGDGTs (6–5.5, 2.8–2.5, and 2–0.2 kyr cal BP) coincide with changes in vegetation in the catchment area, driven by climate and/or human activities. This suggests that vegetation modifications in the watershed impact brGDGT distributions and may thus bias brGDGT-based paleoclimatic reconstructions.

Keywords: Branched GDGTs; soil erosion; anthropogenic impact; vegetation dynamics; altitude lake; Holocene

1. Introduction

Mid-altitude lakes like Lake St Front (Massif Central, France) are subject to extreme environmental conditions which make them particularly sensitive to climatic and landscape changes. Human activities can disturb ecosystems. Deforestation increases runoff and destabilizes soils as does agriculture and pastoralism (e.g., Dearing and Jones, 2003; Lotter and Birks, 2003; García-Ruiz, 2010). These activities thus substantially increase the sediment delivery to lakes through soil erosion by runoff (e.g., Dearing and Jones, 2003). Nutrient inputs to the lakes also increase and can lead to eutrophication of the lake (e.g., Lavrieux et al., 2013a). Multiproxy studies of lacustrine sediments enable the reconstruction of such changes and provide insights into the long-term interactions between earth, climate, and humans (e.g., Birks and Birks, 2006).

The first evidence of human incursion into the Velay region (eastern part of Massif Central; Fig. 1A) dates back to the Mousterian at the beginning of the last glacial period and occurred in the valleys (Philibert et al., 1986; Daugas and Raynal, 1989). Late-glacial and Holocene climatic improvements allowed humans to populate higher altitude regions, predominantly during the Mesolithic and Neolithic (Daugas and Raynal, 1989). Archeological evidence supports the existence of regional settlements in the Massif Central as early as 7.5 kyr cal BP (Georjon et al., 2004; Pouenat, 2007; Macaire et al., 2010) and, more specifically, 6.9 kyr cal BP for the Velay region (Daugas et al., 1983; Miallier et al., 1983). After about 6 kyr cal BP, evidence of human occupation became more frequent. From the Final Neolithic (4.7–3.7 kyr cal BP) and particularly the Ancient Bronze Age (3.7–3.4 kyr cal BP) onward, the archeological and palynological records indicate continuous human occupation and active landscape management (Coûteaux, 1984; Reille, 1992; Miras et al., 2004; Lavrieux et al., 2013a, 2013b).

Proxies based on branched glycerol dialkyl glycerol tetraethers (brGDGTs), biomarkers of bacterial origin, have been recently developed from soil analyses (Weijers et al., 2007). These

compounds are increasingly studied in many environments, particularly in lakes (e.g., Buckles et al., 2014a, 2014b; Miller et al., 2018; Russell et al., 2018). The producers of these bacterial membrane lipids remain mostly unknown except for subdivisions of Acidobacteria (Weijers et al., 2006, 2009; Sinninghe Damsté et al., 2011, 2014, 2018). They are transported via soil erosion through runoff to aquatic systems where they can be preserved in the sediments (e.g., Hopmans et al., 2004). A variety of structures have been identified in brGDGTs including a varying number (0–2) of methyl branches and cyclopentane moieties (0–2; Supplementary Fig. S1). This structural variability is associated with the ability of the brGDGT producers to modify the composition of their cellular membrane lipids in response to specific environmental parameters such as temperature and pH (e.g., Weijers et al., 2007). Two indices were defined: the cyclization ratio of branched tetraethers (CBT), which are correlated with soil pH, and the methylation index of branched tetraethers (MBT) which is correlated to mean annual air temperature (MAAT) and soil pH (Weijers et al., 2007; Peterse et al., 2012). Recently improved chromatography techniques separate the 5-, 6- and 7-methyl (Me) isomers of penta- and hexamethylated brGDGTs which co-eluted with the traditional method (De Jonge et al., 2013, 2014a; Ding et al., 2016). This new technique thus improves the quantification of the different brGDGT forms (De Jonge et al., 2013, 2014a; Ding et al., 2016).

Many lake studies have shown that brGDGT distributions differ between lake sediments and catchment soils (e.g., Tierney and Russell, 2009; Tierney et al., 2012; Wang et al., 2012; Buckles et al., 2014a, 2014b; Russell et al., 2018). These studies suggest production of brGDGTs in water column and/or sediments which hampered paleoclimate reconstructions from lake sediments. Several tools have been developed to determine brGDGT sources and to allow their use as terrigenous input tracers. These include the BIT index (Hopmans et al., 2004), the weighted average number of cyclopentane moieties and the degree of methyl

branching of the brGDGTs (Sinninghe Damsté, 2016), the ΣIIIa/ΣIIa ratio (Xiao et al., 2016) and the stable carbon isotope composition ($\delta^{13}C$) of brGDGTs (e.g., Weber et al., 2015, 2018). Among these tools, the BIT index and the $\delta^{13}C$ of brGDGTs were already applied for lake studies (e.g., Niemann et al., 2012; Colcord et al., 2017), but the tools recently proposed by Sinninghe Damsté (2016) and Xiao et al. (2016) were developed in the oceanic realm and their applicability in lakes has yet to be tested. Many studies have demonstrated the impact of human activities on bacterial and phytoplanktonic communities (e.g., Moon et al., 2016; Murphy et al., 2016; Lambert et al., 2018), but fewer studies have considered the potential direct and indirect impacts of human occupation and activities on GDGT distributions (Das et al., 2012; Naeher et al., 2014; dos Santos and Vane, 2016; Chen et al., 2018; Song et al., 2018).

Palynological reconstructions are extensively used to reconstruct past environmental changes (e.g., Reille and de Beaulieu, 1990) at a regional and at the local scale. As vegetal taxa are adapted to specific climate conditions, pollen assemblages can give information on climate changes (e.g., Birks et al., 2011; Gambin et al., 2016). Anthropogenic disturbances can be demonstrated thanks to some specific markers like changes in the sum of arboreal pollen and the rate of cultivated, ruderal and nitrophilous plants (e.g., Lavrieux et al., 2013b; Shumilovskikh et al., 2016).

We studied Lake St Front, a maar located at an altitude of 1230 m in the eastern Velay region (Massif Central, France), in a climatic transition zone between Atlantic and Mediterranean influences. It has a small catchment area and a high potential for the accumulation and preservation of sedimentary organic matter due to a relatively high sedimentation rate. A 65 m depth core was recovered from the lake in 1991 which contained deposits dating back to the penultimate glacial cycle (i.e., between 130 and 180 kyr BP; Vlag et al., 1997). Due to human occupation of the immediate surroundings of Lake St Front since

the Neolithic (e.g., Dendievel, 2012 and References therein), this study site offered a good opportunity to test the anthropogenic impacts on brGDGT distributions.

We identified and quantified the brGDGTs present in the catchment soils and in the Holocene sedimentary sequence of Lake St Front in order to: (1) determine the sources of brGDGTs present in modern lake sediments using the available source indices and by comparing the brGDGT distributions between catchment soils and lake sediments, and (2) reconstruct the changes in brGDGT sources during the Holocene in relation to vegetation changes and anthropogenic impacts.

2. Material and methods

2.1. Site description

Lake St Front (44°58' N, 4°10' E, 1234 m) occupies a sub-circular crater located on the Meygal-Mézenc plateau (eastern Velay, Massif Central, France; Fig. 1A). The crater was cut through Quaternary basalts by a phreatomagmatic explosion (maar: Mergoil, 1987; Teulade et al., 1991). The lake diameter is 600 m and its maximum depth is 6 m. The 1.5 km^2 lake catchment area (Fig. 1B) contains numerous streams. Currently, the two main environment types are coniferous and deciduous forests with *Pinus sylvestris* and *Quercus pubescens* dominant (Carles, 1956) and grassland areas that are used as cattle pasture (Fig. 1B and 1C). A peat bog located on the northern shore documents high lake level deposits dating from the Holocene (Florschutz, 1954; Bout, 1973). The lake is eutrophic and, apart from rainfall/runoff, it is supplied by surface and probably groundwater springs fed by a groundwater table located at around 20 m (Mergoil et al., 1993). A small outlet was dug in recent historical times at the southwestern shore to control the lake water level.

Mean annual temperature ranges from 6 °C to 9 °C with a mean value of 7 °C. Average winter temperature is 1 °C and average summer temperature is 15 °C with daily maxima that

can exceed 25 °C. The average annual precipitation is 1000 mm. Rainfall originates from Atlantic or Mediterranean humid air masses pushed by winds. Snowfall occurs more than 50 days per year on the Eastern Velay plateau. The lake is usually frozen for at least three months each year (Fillod, 1985). Modern climatic parameters were obtained from the instrument database of Météo-France (https://donneespubliques.meteofrance.fr) at the nearby (11 km) station of Mazet-Volamont and the nearest altitude (1130 m) for the period 2009–2017. Data for longer periods were from the stations of Saint Julien Chapteuil (distance 9 km, altitude 810 m, period 1995–2017) and Le Puy en Velay (distance 22 km, altitude from Lake St Front to the northwest, 833 m, period 1981–2010). Temperature values were corrected using an altitudinal gradient of 0.6 °C/100 m (Gandouin et al., 2016).

Lake St Front presents ideal conditions to provide continuous sedimentary records for the last climatic cycle. It has a shallow bathymetry allowing water column mixing by the wind, a simple food-web system and a relatively simple limnology. Archeological evidence shows human presence in the immediate surroundings of Lake St Front since the Neolithic (e.g., Dendievel, 2012 and References therein). This relatively simple system in a temperate climate was appropriate for the study of brGDGTs and the potential impact of anthropogenic activities on their distribution.

2.2. Sampling

Lake sediment cores were recovered during two coring campaigns in 1991 and 2016 (Fig. 1B, Table 1). In 1991, three parallel cores SFA, SFB, and SFC were collected down to depths of 45 m, 65 m, and 18 m, respectively (Rhoujjati, 1995). Piston core sections of 1 m length and 8 cm diameter were recovered from the top 35 m of the SFA core and from the top 22 m from both the SFB and SFC cores. Since their collection, the cores were stored refrigerated and no significant alterations have been detected (Supplementary Text 1 and

Supplementary Fig. S2). For this study, a composite sequence was reconstructed from cores SFB and SFC.

Additional cores were collected during July 2016 using UWITEC equipment (corers and coring platform) with the 2 m long hammer piston corer at sites SF16-2 (19 m) and SF16-3 (13 m; Fig. 1B). They were used to fill the hiatus of the SF-1991 cores (Andrieu et al., 1995) and to obtain a continuous composite sequence. A 60 cm gravity core was collected across the water–sediment interface in the central part of the lake (SF16-1A; Fig. 1B), while other shallow interface cores (50 cm maximum depth) were recovered from several shoreline sites (Fig. 1B, Table 1). Soil samples (2–5 cm depth), upper sediments of catchment streams (0–2 cm depth), and shoreline surface sediments were also collected from around the lake (Fig. 1B, Table 1).

2.3. Core description and preliminary analyses

We focused on the upper 13 m long part of the core covering the Holocene. The sediment sequence consisted of organic "gyttjas", an accumulation of vegetable fibers packed into a clay matrix that is formed under temperate climatic conditions by autochthonous organic matter (OM) and soil degradation products (Fig. 2; Rhoujjati, 1995). This top organic unit contained dissolved gas formed by OM degradation and possibly by deep gas sources of volcanic origin.

In the field, low field magnetic susceptibility (MS) was measured at 2 cm intervals using the MS2 Bartington susceptibilimeter connected to a 90 mm diameter MS2C probe, enabling correlations with the MS profiles between the SF-2016 and SF-1991 cores (Vlag et al., 1996, 1997). Magnetic susceptibility is a dimensionless quantity expressed in SI units. Matter can become magnetized under the influence of a magnetic field. In volcanic geological contexts, where magnetite and titanomagnetite are the main ferrimagnetic minerals present, MS mainly

measures the concentration of these magnetic minerals in the sediment mixture. This reveals physical and/or chemical conditions from the erosion to the diagenesis that are related to the environment and/or climate.

2.4. Age model

The age control of the upper 20 m of the sequence was performed with radiometric methods. Lead-210 (^{210}Pb) activity was measured in the upper 30 cm of the composite sequence at GEOTOP Montreal (Table 2, Fig. 2B). The constant flux constant sedimentation model (CFCS), a particular case of the constant initial concentration model (CIC) (Ghaleb, 2009), was used to interpret the ^{210}Pb profile. AMS ^{14}C dating of total OM and organic macrofossils was carried out on an ARTEMIS accelerator mass spectrometer (Gif-sur-Yvette, France). Five radiocarbon age estimates (Table 3, Fig. 2A) were available on the SFA core from Rhoujjati (1995). We added nine ^{14}C age estimates on the SFB and SFC cores (Table 3, Fig. 2A). Twenty ^{14}C age estimates were obtained for SF16-2 and SF16-3 cores (Table 3, Fig. 2A). Radiocarbon age estimates (^{14}C year BP) were converted to calendar years before 1950 (cal yr BP) using the IntCal13 calibration curve (Reimer et al., 2013). The age model was developed using the Bayesian model of the Bacon program (version 2.2; Blaauw and Christen, 2011) implemented in R (version 3.3.2; R Development Core Team, 2015). Ages were interpolated using the weighted mean within a 95% confidence interval.

2.5. Pollen analyses

Pollen analyses were conducted on 107 samples from the SFA profile (Supplementary Table S1). Pollen and spores were extracted using a flotation liquor (d = 2; Nakagawa et al., 1998). Identification of sporopollen material was carried out using a photonic microscope at 500× magnification. Standard palynological identifications were based on the pollen reference

collection of the Institut Méditerranéen de Biodiversité and Marine and Continental Ecology (CNRS, Aix-en-Provence, France) and pollen photographic atlases (Reille, 1992, 1995, 1998; Beug, 2004). Pollen percentages were calculated based on a pollen sum (PS) including all plants except for aquatics, ferns, and bryophytes. Different assemblages of taxa were considered in this study. The arboreal pollen sums all the tree taxa and among these taxa, two ensembles were distinguished, the thermophilous and mesophilous trees. The taxa included in the thermophilous forest were *Acer*, *Corylus*, *Hedera*, *Ilex*, *Lonicera*, *Ostrya*, deciduous *Quercus*, *Quercus ilex* t., *Pistacia*, *Sambucus*, *Sorbus*, *Tilia*, *Ulmus*, *Viburnum* and *Viscum*. The taxa forming the mesophilous forest were *Abies*, *Carpinus* and *Fagus*. The anthropogenic taxa linked with human occupation and activities were also studied and separated into three groups. The nitrophilous taxa associated with farming were *Plantago lanceolata*, *P. major*, *Rumex*, Chenopodiaceae and *Urtica*; the cereals, markers of agriculture, included Cerealia and *Secale* and the pollen of *Juglans* was representative of arboriculture.

2.6. BrGDGT analysis

The sedimentary sequence was sampled at 10 cm increments and stored in a freezer prior to being freeze-dried and powdered. Before powdering, soils and interface samples were sieved to remove macro-remains and roots. After adding the internal standard C_{46} GDGT (Huguet et al., 2006), the lipids from 1–2 g of each sample were extracted using the accelerated solvent extraction method (ASE 350 Dionex system) with dichloromethane (DCM):methanol (MeOH) (90:10, v/v) at 120 °C and 80–100 bar. The total lipid extracts were then separated into apolar and polar fractions using Al_2O_3 columns and hexane:DCM (1:1, v/v) and MeOH:DCM (1:1, v/v) to eluate, respectively, the apolar and polar fractions following the method described by Sanchi et al. (2013). Polar fractions were analyzed with high-performance liquid chromatography–atmospheric pressure chemical ionization-mass

spectrometry (HPLC–APCI-MS) using an Agilent 1260 Infinity HPLC coupled to an Agilent 6120 quadrupole mass spectrometer following the new method described by Hopmans et al. (2016) with the modifications reported by Davtian et al. (2018). The analyses were carried out at the CEREGE (Aix-en-Provence, France).

Soil and sediment samples were run at least in duplicate. Peak areas of GDGTs were determined by manual integration of the peak areas of $[M + H]^+$ ion traces of GDGTs (*m*/*z* 1292.3, 743.7, 1050.0, 1048.0, 1046.0, 1036.0, 1034.0, 1032.0, 1022.0, 1020.0, 1018.0 according to Davtian et al., 2018; Supplementary Table S2) using the Agilent Chemstation chromatography management software. GDGT concentrations were obtained by relating chromatogram peak areas to the known concentration of the internal standard C_{46} GDGT (Huguet et al., 2006, Supplementary Table S2). The relative response factor (RRF; Huguet et al., 2006) was inferred by running mixed samples of C_{46} and GDGT-0 (caldarchaeol, 1:1). One sample was chosen as an external standard and was run at the beginning and at the end of each batch to test the reproducibility for instrument drift.

2.7. Statistical analysis and calculation of brGDGT-based indices

We used CoDaPack software (version v2) to perform compositional analyses (Comas-Cufí and Thió-Henestrosa, 2011). This method accounts for the compositional nature of geochemical data which are constrained as their sum is equal to 1 (100%), using the Aitchison geometry (Aitchison, 1986). This geometry works into the simplex SD, a generalization to D dimensions of the ternary diagram concept (D = 2; Aitchison, 1986). Log-ratio techniques transfer the information from the simplex to a Euclidian space where standard non-constrained multivariate statistics can be used while conserving the relationship between the components (Aitchison, 1986; Filzmoser and Hron, 2011; Pawlowsky-Glahn and Buccianti, 2011; Reimann et al., 2012; van den Boogaart and Tolosana-Delgado, 2013; McKinley et al.,

2016). Prior to performing principal component analysis (PCA), we applied the centred log-ratio (clr) transformation (Aitchison, 1986; McKinley et al., 2016). All the other statistical tests were performed using R (version 3.3.2; R Development Core Team, 2015) and PAST software (version 3.04; Hammer et al., 2001).

Several indices were calculated using the relative abundances of brGDGTs which correspond to the proportion of each brGDGT compared to the sum of all brGDGTs. Roman numerals in the following equations refer to the different brGDGT forms described in Supplementary Fig. S1.

We measured crenarchaeol to determine the branched and isoprenoid tetraether index (BIT) values, using a modified version of the definition by Hopmans et al. (2004) to include the 6-, 7- and 5/6-Me forms (De Jonge et al., 2014a; Weber et al., 2015; Ding et al., 2016), which are denoted as X′, X_7 and IIIa′′, respectively:

$$\mathrm{BIT} = \frac{\mathrm{Ia} + \mathrm{IIa} + \mathrm{IIIa} + \mathrm{IIa'} + \mathrm{IIIa'} + \mathrm{IIIa''} + \mathrm{IIa_7} + \mathrm{IIIa_7}}{\mathrm{Ia} + \mathrm{IIa} + \mathrm{IIIa} + \mathrm{IIa'} + \mathrm{IIIa'} + \mathrm{IIIa''} + \mathrm{IIa_7} + \mathrm{IIIa_7} + \mathrm{Crenarchaeol}} \qquad (1)$$

The BIT index allows evaluation of the proportion of terrigenous brGDGTs present in sediments and varies from 1 in soils to 0 in open oceans (Hopmans et al., 2004).

To determine brGDGT sources, the proportions of tetra- (I), penta- (II) and hexa- (III) methylated brGDGTs were calculated using the fractional abundances of brGDGTs following Sinninghe Damsté (2016) and including the 5/6- and 7-Me forms (Weber et al., 2015; Ding et al., 2016). We also calculated the weighted average number of cyclopentane moieties following Sinninghe Damsté (2016).

The ΣIIIa/ΣIIa ratio was determined to identify brGDGT sources following the definition of the IIIa/IIa ratio by Xiao et al. (2016) who combined the 5- and 6-Me forms to correspond to the traditional chromatography techniques which did not separate these isomers. In accordance with this definition, we included the 5/6- and 7-Me forms as:

$$\sum IIIa/\sum IIa = \frac{IIIa + IIIa' + IIIa'' + IIIa_7}{IIa + IIa' + IIa_7} \quad (2)$$

We modified the annotation of the IIIa/IIa ratio defined by Xiao et al. (2016) to clarify that it takes into account all the isomers of the brGDGTs IIIa and IIa.

The reproducibility of replicates from the external standard measured on different days was 0.004 for the BIT index and 0.01 for the ΣIIIa/ΣIIa.

The isomer ratio (IR) represents the relative amount of the 6-Me or 7-Me penta- and hexamethylated with respect to the total corresponding 5-Me, 6-Me, 5/6-Me, and 7-Me penta- and hexamethylated brGDGTs and was calculated using a modified version of the definition by De Jonge et al. (2014b):

$$IR_{6Me} = \frac{IIa' + IIb' + IIc' + IIIa' + IIIb' + IIIc'}{\Sigma\text{pentamethylated brGDGTs} + \Sigma\text{hexamethylated brGDGTs}} \quad (3)$$

$$IR_{7Me} = \frac{IIa_7 + IIIa_7 + IIIb_7}{\Sigma\text{pentamethylated brGDGTs} + \Sigma\text{hexamethylated brGDGTs}} \quad (4)$$

These isomer ratios allow comparison of the relative abundances of the different isomers; the lower the ratio's value, the lower the fractional abundances of the considered isomer compared to the other isomers.

3. Results

3.1. Age-depth model

^{210}Pb activity decreased steadily with depth in the upper 30 cm except for the top 0.5 cm (Table 2). The estimated sedimentation rate was 0.37 $\pm$ 0.05 cm/yr. This result is consistent with the rate of 0.40 cm/yr obtained from ^{14}C measurements in the upper 5 m.

The sedimentation rate increased slightly during the Holocene (from 0.04 to 0.4 cm/yr) with an average value of 0.33 cm/yr. Two peaks were recorded at 5.5 kyr cal BP and between 1.4 and 2 kyr cal BP with means of 1.0 and 1.6 cm/yr, respectively (Fig. 2D). The average

temporal resolution for the brGDGT analyses was 90 years, 100 years for pollen counts and 28 years for magnetic susceptibility measurements.

Age estimates obtained from ^{14}C and ^{210}Pb measurements for the upper core yielded a discrepancy of around 800 years with ^{14}C providing an older age estimate (Tables 2 and 3). Plant macrofossils and bulk sediment from 1.90 m showed an offset of only 200 years (Table 3). Thus, the reservoir effect is not constant over time which precludes application of a constant correction factor.

3.2. Modern brGDGT distribution in Lake St Front sediments and catchment soils

All the brGDGTs described thus far, including 7-Me brGDGTs (see Supplementary Text 2), were present in both catchment soils and surface sediments (0–10 cm) of Lake St Front, except for brGDGT IIIa″ which was not detected in soils (Fig. 3). The summed concentrations of brGDGTs ranged from 0.8 to 29 μg/g in soils (mean = 7 μg/g) and from 1 to 15 μg/g in lake sediments (mean = 6 μg/g, Tables 4 and 5). While brGDGTs without cyclopentane moieties (brGDGTa, 88% for soils and 83% for sediments) and pentamethylated brGDGTs (II, 48% for both soils and sediments) were dominant in both surface sediments and catchment soils, the fractional abundances of the other brGDGTs exhibited a different pattern (Fig. 3, Table 4). Soils contained higher abundances of tetramethylated brGDGTs (I, 34%) than sediments (19%), and in particular brGDGT Ia (28% vs 14%, respectively). Sediments contained higher abundances of hexamethylated brGDGTs (III, 33%) than soils (18%), especially for brGDGT IIIa′ (11% vs 4%, respectively). The relative abundance of pentamethylated brGDGTs was similar for both soils and sediments, but brGDGT IIa was more abundant in soils (35%) than in sediments (22%) while brGDGT IIa′ was more abundant in sediments (13%) than in soils (8%). The distribution patterns of the 5- and 6-Me forms also differed in that the relative abundance of 6-Me over 5-Me brGDGTs (IR_{6Me})

ranged from 0.03 to 0.3 in soils (average of 0.19) and from 0.3 to 0.4 in sediments (average of 0.36, Table 4). IR_{7Me} was significantly higher in sediments (0.05) than in soils (0.02, Table 4, *t*-test $p < 0.0001$). The BIT index was very close to 1 in sediments and soils (Fig. 3). The ΣIIIa/ΣIIa values ranged from 0.2 to 0.6 in soils (average = 0.4, Fig. 3, Tables 4 and 5) and from 0.6 to 1 in lake sediments (average = 0.8).

The first axis of the covariance biplot (not shown), computed after a clr-transformation of the dataset, explained 96% of the variance in the dataset and is linked to the presence or absence of brGDGT IIIa″. In a second compositional analysis where brGDGT IIIa″ had been removed, the two principal components (PC) explained 66 and 15% of the variance. BrGDGTs Ia, IIa, and IIIa scored positively on PC1 whereas the 6- and 7-Me forms, except IIa′, scored negatively (Fig. 4A). Considering the sample scores on PC1 and PC2, soils and sediments appeared to form two separated groups, scoring positively and negatively on PC1, respectively (Fig. 4B). Scores for catchment samples were more heterogeneous than for sediments, despite minor differences between cores.

We observed three groups in the compositional analysis (Fig. 4B). The first group corresponded to samples collected in deciduous forest (S2a and S2b, Table 1) and was distinct from the other two groups by its low negative values on PC2 and its maximum on PC1; the second group corresponded to samples collected in coniferous forests (S1a and S1b), streams, and grassland (except S3a) and had intermediate values on PC2; the third group contained samples collected in the peat bog, the marsh, streams, and the grassland sample S3a, and exhibited high values on PC2 and relatively lower values on PC1. Grassland samples were spread across the last two groups. The waterlogged soils formed a cluster with streams (S4, S7, S3a and S3b, and the streams R1–R5) and scored positively on PC2 while all the other soils (except sample S6) scored negatively (Fig. 4B).

Considering the surface sediments only (0–3 cm), the differences between cores were smaller for all cores except for the G core. Samples D1a and D1b, corresponding to surface sediments from the lake's water edge, and sample 1A-55 had slightly less-negative scores on PC1 than the other sediment samples (*t*-test $p < 0.0001$) and was set apart from the group of the other sediment samples (Fig. 4B).

3.3. Sedimentological, geochemical, and palynological evolution through time

Magnetic susceptibility (MS) at the beginning of the Holocene presented relatively high values (47.10^{-5} SI units) which decreased rapidly to 0 SI units (Fig. 5B). MS slightly increased around 7 and 6 kyr cal BP before decreasing to negative values. MS slightly increased from 2.5 kyr cal BP, then abruptly from 1.8 kyr cal BP and remained high until 0.2 kyr cal BP (until 36.10^{-5} SI units, Fig. 5B).

Through the Holocene and until 2 kyr cal BP, the Arboreal Pollen (AP, see Section 2.5 for definition) percentages remained at an almost constant high level (near 90% of the pollen sum, PS; Fig. 5D and Supplementary Table S1), except for a decrease from 7.3 to 5.5 kyr cal BP (minimum of 64% of PS reached at 6.7 kyr cal BP). At about 2.8 kyr cal BP, AP values rapidly decreased by almost 50% in as little as 1000 years (Fig. 5D and Supplementary Table S1). The thermophilous tree pollen (see Section 2.5 for definition) was dominant at the beginning of the Holocene (80% between 10.1 and 8 kyr cal BP but decreased rapidly to reach 20% by 5 kyr cal while mesophilous tree pollen (see section 2.5 for definition) percentages increased rapidly from 6.3 kyr cal BP to reach 50% of the PS by 5.5 kyr cal BP (Fig. 5D and Supplementary Table S1). Except for some high values at the beginning of the Holocene, which corresponded to steppe plants and were not linked to anthropogenic activity, the pollen values of anthropogenic taxa (see Section 2.5 for definition) remained very low

until 2.8 kyr cal BP after which they increased rapidly to reach 16% by 200 yr cal BP (Fig. 5E and Supplementary Table S1).

The BIT index remained very close to 1 during this period (average of 0.998 ± 0.001, Fig. 5G). However, its value slightly increased at the beginning of the Holocene (0.995 to 0.998 at 10.9 kyr cal BP) and then values slightly decreased until 8.9 kyr cal BP prior to increasing again until 2 kyr cal BP with a rapid drop at 5.5 kyr cal BP (0.993). From 2 kyr cal BP, the values of the BIT index decreased with two abrupt drops at 1.8 and 0.1 kyr cal BP (Fig. 5G).

The fractional abundance of IIIa″ fluctuated between 0.2% and 3.5% through the Holocene (Fig. 5H). The relative abundance of IIIa″ decreased during the beginning of the Holocene (to 0.6% at 10.9 kyr cal BP). Then, the values increased to reach their maximum at 8.6 kyr cal BP. From 8.3 kyr cal BP, fractional abundances decreased abruptly to stabilize around 1.2% before decreasing again from 4.2 kyr cal BP (Fig. 5H, Supplementary Table S2).

The ΣIIIa/ΣIIa ratio fluctuated between 0.52 and 1.16 during this interval (Fig. 5I). Its value decreased from the beginning of the Holocene until 5.9 kyr cal BP (from 1.16 to 0.53) with a rapid drop at 5.9 kyr cal BP (–0.19). Then, the ratio values increased until 5.1 kyr cal BP and decreased again until 2.7 kyr cal BP when they abruptly dropped and reached their minimum prior to a rapid increase until 2 kyr cal BP (to 0.87). The values again dropped abruptly and remained low before increasing from 0.2 kyr cal BP.

4. Discussion

4.1. Heterogeneity of catchment samples

We found a large diversity of brGDGT distribution patterns in the catchment area. On a global scale, brGDGT distribution is correlated with air temperature and soil pH (e.g., Weijers et al., 2007; De Jonge et al., 2014a). The restricted sampling area (1.5 km^2) leads to

minimal spatial air temperature variations. The diversity of brGDGT distribution patterns may reflect the different environment types found there: coniferous and deciduous forests, grassland used as cattle pasture, peat bog, and marsh (Figs. 1 and 4B; Weijers et al., 2011; Ayari et al., 2013; Huguet et al., 2013; Naeher et al., 2014; Liang et al., 2019). Nonetheless, the variability observed, even within each type of environment, suggests that this factor may not have the greatest influence (Weijers et al., 2010; Buckles et al., 2014b).

The proximity of high water content samples on PCA (Fig. 4B) and their brGDGT distributions similar to sediments (Table 5) suggests that soil water content may be an additional factor influencing brGDGT distributions (Weijers et al., 2010; Loomis et al., 2011; Buckles et al., 2014b; Naeher et al., 2014; Dang et al., 2016). However, Dang et al. (2016) found an opposite tendency in brGDGT distributions in humid soils (higher brGDGT I abundance and lower brGDGT III abundance), which suggests that water content may not be the most determinant factor of brGDGT distribution. Instead, pH is a better candidate to explain the diversity of brGDGT distribution patterns observed in catchment samples.

4.2. Significant brGDGT in situ production in the lake

Numerous studies have reported discrepancies in brGDGT distributions between surface sediments and soils (Tierney et al., 2010; Loomis et al., 2011, 2014; Sun et al., 2011; Wang et al., 2012; Buckles et al., 2014a, 2014b; Günther et al., 2014; Naeher et al., 2014; Hu et al., 2015; Cao et al., 2017), suggesting that in situ production can occur in a wide range of lacustrine environments. The main distinguishing feature for brGDGT distributions between catchment samples and sediments in Lake St Front is the presence of brGDGT IIIa″ only in the latter (Fig. 3). The brGDGT IIIa″ has never been found above detection limits in soils (De Jonge et al., 2014a; Weber et al., 2015, 2018) which suggests that this brGDGT results from in situ production in the lake (Weber et al., 2015). In situ production is also evidenced by the

clustering on PCA (Fig. 4B) revealing different overall brGDGT distribution patterns between surface sediments and catchment samples (lower abundances of brGDGT I, higher abundances of brGDGT III, and higher IR_{6Me} and IR_{7Me} in sediments than in soils; Fig. 3, Table 4). The brGDGT distribution pattern in sediments in Lake St Front is consistent with those found in cold lakes (Sun et al., 2011; Zink et al., 2016) and some Chinese lakes (Dang et al., 2018).

Additional evidence for the in situ production of brGDGTs is provided by the relative homogeneity of the surface sediment group, which contrasts with the heterogeneity of the soil signatures in the catchment area (Fig. 4B). A locally higher proportion of detrital inputs gave a brGDGT signature slightly different in three surface and sub-surface sediment samples which was illustrated by the lower value of the ΣIIIa/ΣIIa ratio (1A-55, D1a and D1b; Fig. 4B, Table 5).

Preferential transport or degradation seem unlikely since similar chemical structures probably have similar degradation rates (Schouten et al., 2004; Xiao et al., 2016). BrGDGTs share the same molecular structures with only minor variations and thus they should have similar degradation rates. This assumption was confirmed by a thermal degradation experiment (He et al., 2012) which showed a decrease of brGDGT concentrations with increasing temperature without a change in relative abundances. So, despite the low surface and shallow depth of Lake St Front, in situ production of brGDGTs is significant and confirms the necessity of testing for brGDGT origin in all lake studies.

4.3. Test of the existing tools to discriminate brGDGT sources

A comparison of brGDGT distributions in soils and sediments leads to the conclusion that there is in situ production in Lake St Front. We compared these results with those of the existing tools for brGDGT source determination. The weighted average number of

cyclopentane moieties for the brGDGTs I and II of our soil and sediment samples did not exceed 0.4, which corresponds to the range of values of global soils. This indicates a terrigenous source for branched tetraethers present in sediments (Sinninghe Damsté, 2016; Table 5). The degree of methyl branching of the brGDGTs in our samples supports the same conclusion: the fractional abundances of tetra-, penta- and hexamethyl brGDGTs correspond with those in global soils (Sinninghe Damsté, 2016; Table 5). The tools developed in the marine realm by Sinninghe Damsté (2016) do not discriminate sediments and soils of Lake St Front, possibly due to the reduced size of the watershed and the shallow depth of the lake which guarantee very similar conditions for brGDGT-producing bacteria.

The BIT index values in surface sediments (0–10 cm) were close to 1 (Table 5) indicating that brGDGTs predominate over crenarchaeol. This also denotes a prevailing terrigenous source of branched tetraethers in Lake St Front sediments or a water depth that is too shallow for crenarchaeol production (Tierney et al., 2010; Wang et al., 2019). However, the use of the BIT index as a tool to discriminate brGDGT source is questioned, in particular due to the existence of in situ production (e.g., Sinninghe Damsté, 2016).

All existing GDGT source indices point to a terrigenous source of brGDGTs except the ΣIIIa/ΣIIa ratio which suggests a mixed origin. Xiao et al. (2016) used this ratio to distinguish brGDGT origins. When comparing soils and marine sediments, 90% of the soils from the global soil database had a ratio lower than 0.59 and 90% of the marine sediments tested had a ratio higher than 0.92. While the ΣIIIa/ΣIIa ratio has never been used in the lacustrine realm (Xiao et al., 2016), it offers a contrasting picture when soil and lake samples are considered and provides evidence for the mixed origin of brGDGTs in surface sediments. The catchment samples exhibited values below the limit for terrigenous origin, except the stream sample R3 which showed slightly higher values, while surface sediment samples

showed values above the soil limit and below the limit for aquatic origin consistent with a mix of aquatic and soil production (Table 5).

In the modern situation, brGDGTs in Lake St Front sediments have thus a mixed origin: aquatic and terrigenous. Analysis of catchment samples and surface sediments revealed that their brGDGT distribution patterns were significantly different. This constitutes a major problem for paleotemperature reconstructions. In fact, such reconstructions rest on the use of two indices, the methylation index of branched tetraethers (MBT) and the cyclization ratio of branched tetraethers (CBT) calculated from the brGDGT abundances (see Supplementary Text 3). In sediments, the mixing of brGDGTs of distinct origins characterized by significantly different brGDGT distribution patterns can thus introduce a bias in paleotemperature reconstruction (see Supplementary Fig. S3 and Supplementary Text 3). Prior to any attempt of paleotemperature reconstruction from brGDGTs in lake sediments, it is necessary to determine the brGDGT origin and if mixed origin is detected, to evaluate the proportion of each source to correct the bias. In the present situation, the ΣIIIa/ΣIIa ratio appears to be the single tool based on brGDGT abundances able to discriminate soil and aquatic sources. It can thus be applied in the past to reconstruct past changes of brGDGT sources.

4.4. Evolution of brGDGT sources during the Holocene

We compared the ΣIIIa/ΣIIa values with the C/N ratio, an established tool for determining organic matter origins (e.g., Stein and Littke, 1990). The decrease of ΣIIIa/ΣIIa along the sedimentary sequence, consistent with the other proxies, indicated an increase in the proportion of terrigenous material (Fig. 5). Vegetation cover development (continuous increase of AP percentage, Fig. 5D) and soils limited the erosion of the magmatic bedrock (decrease of magnetic susceptibility; Fig. 5B) and enhanced organic matter (OM) production

(increase of Total Organic Carbon, TOC, 10.5% to 26%; Rhoujjati, 1995). The forest cover also enhanced bacterial community development. During the Early Holocene, the lake became eutrophic and primary production increased as indicated by xanthophyll blooms (Rhoujjati, 1995) and high abundances of IIIa″ (Fig. 5H). The proportion of terrigenous OM quickly increased compared to lacustrine OM which was illustrated by the decrease of ΣIIIa/ΣIIa and increase of C/N (Rhoujjati, 1995) until the values of both ratios moved out of the aquatic production realm (ΣIIIa/ΣIIa < 0.92 and C/N > 10; Fig. 5F and 5I; Stein and Littke, 1990).

The overall trend of increasing terrigenous inputs was interspersed by three abrupt events from 6 to 5.5, 2.8 to 2.5, and 2 to 0.2 kyr cal BP which were characterized by a sharp decrease in ΣIIIa/ΣIIa below the limit for a soil origin and a decrease in the fractional abundance of IIIa″ (Fig. 5H and 5I). These events seem to correspond to higher terrigenous inputs as indicated by the higher sedimentation rate, MS, and TOC (Fig. 5A–C; Rhoujjati, 1995) and an increase in primary production (i.e., lower C/N and BIT index, in conjunction with higher ΣIIIa/ΣIIa and fractional abundances of IIIa″, Fig. 5F–I; Rhoujjati, 1995) that followed each decrease in ΣIIIa/ΣIIa.

The variation in the ΣIIIa/ΣIIa ratio suggests that the brGDGT sources drastically changed throughout the Holocene. In the late Younger Dryas, brGDGTs were mainly of lacustrine origin (high ΣIIIa/ΣIIa values and fractional abundances of IIIa″, Fig. 5H and 5I) while during the Late Holocene they mostly originated from the catchment area. These source changes led to changes of the brGDGT distributions which could, by analogy with present situation (see Supplementary Fig. S3 and Supplementary Text 3), bias paleoclimatic reconstructions based on brGDGTs. Thus, it is necessary to test for brGDGT source changes in the past.

4.5. Significance of the ΣIIIa/ΣIIa ratio as a proxy for brGDGT origin

The ΣIIIa/ΣIIa ratio compares the abundances of the brGDGTs containing two methyl groups (hexamethylated forms) with brGDGTs containing one methyl group (pentamethylated forms) and so, it reflects the number of brGDGT methyl groups. Weijers et al. (2007) and Peterse et al. (2012) found a positive correlation between the mean annual air temperature (MAAT) and the methyl indices of brGDGTs (MBT and MBT′). The MBT index corresponds to the proportion of brGDGTs without a methyl group (tetramethylated forms) compared with all forms and reflects the number of methyl groups of the brGDGTs. In contrast, using the global soil database from Peterse et al. (2012), we found a weak negative correlation between ΣIIIa/ΣIIa and MAAT ($R^2 = 0.17$, $n = 272$, $p < 0.0001$; Supplementary Fig. S4). This correlation was mainly due to several MAAT values that were > 20 °C. By removing these values, the correlation was much weakened ($R^2 = 0.05$, $n = 227$, $p = 0.0006$). In conclusion, we found that for soils in temperate climates like Lake St Front there was a very weak correlation between ΣIIIa/ΣIIa and temperature.

To test this correlation in other sediments, we used the global marine database of Xiao et al. (2016). As the sea surface temperatures are not provided in the database, we used latitude since latitude is strongly linked with water and air temperature. Considering all the sediments of the database, the negative correlation between ΣIIIa/ΣIIa and latitude is relatively weak ($R^2 = 0.16$, $n = 1261$, $p < 0.0001$). Considering only surface and sub-surface sediments, the correlation was weaker ($R^2 = 0.03$, $n = 271$, $p = 0.008$). The values of the ΣIIIa/ΣIIa in marine sediments were weakly correlated with latitude and so with water and air temperature.

We also tested the correlation in lakes using available data from modern surface sediments in lakes (Tierney et al., 2010; Loomis et al., 2011, 2012, 2014; Wang et al., 2012; Günther et al., 2014; Li et al., 2016; Zink et al., 2016; Dang et al., 2018; Russell et al., 2018; Weber et al., 2018; Ning et al., 2019; Supplementary Table S3). Considering all the sediments of the database, we obtained a weak but significant negative correlation between ΣIIIa/ΣIIa

and MAAT (R^2 = 0.35, n = 359, p < 0.0001; Supplementary Fig. S4). Once again, this correlation seems to be mainly due to several MAAT values that were >20 °C, the correlation became weaker when removing them (R^2 = 0.23, n = 269, p < 0.0001). Furthermore, the occurrence of in situ production introduces significant variability which seems linked with different mixing percentages of soil and aquatic brGDGT sources rather than with MAAT. The correlation between ΣIIIa/ΣIIa and MAAT for sediments from lakes with in situ production of brGDGTs is very weak (R^2 = 0.04, n = 128, p = 0.02). Shifts in brGDGT sources in temperate environments leads to ΣIIIa/ΣIIa variations more important than ΣIIIa/ΣIIa variations due to temperature changes as the slope of the correlation with temperature is very small and the temperature change during the Holocene limited to a few degrees (e.g., Marcott et al., 2013; Pei et al., 2017).

Furthermore, lake sediment ΣIIIa/ΣIIa ratios show a good correlation with C/N (R^2 = 0.51, n = 135, p < 0.0001), which is also a source indicator, showing that the ΣIIIa/ΣIIa ratio effectively reveals the changes of brGDGT sources (Supplementary Fig. S5 and Supplementary Text 4). The correlation between ΣIIIa/ΣIIa and the fractional abundance of IIIa″, an indicator of the proportion of in situ production, is weaker but still significant (R^2 = 0.32, n = 143, p < 0.0001). While IIIa″ may be a reliable indicator for the occurrence of in situ production, it is not an ideal indicator for the proportion of in situ production compared with soil production. IIIa″ had high variability which may be due to a variable production rate or stem from analytical bias as this brGDGT was only present in low concentrations making its detection and quantification subject to greater error.

Threshold values used to distinguish aquatic, mixed and soil production domains were proposed by Xiao et al. (2016). The value for the soil was obtained from the global database of soil and can thus be used confidently here. However, the value used for aquatic production

was based on marine sediments and the actual lake values might differ. This should be tested for the use of ΣIIIa/ΣIIa to make quantitative assessment of terrigenous brGDGT proportions.

The influence of temperature on the ΣIIIa/ΣIIa ratio of lake sediments in temperate environments seems too weak to have significantly modified the values of the ratio during the Holocene. Shifts in brGDGT sources have a stronger influence on ΣIIIa/ΣIIa values. The variations of the ΣIIIa/ΣIIa ratio observed in Lake St Front sediment through the Holocene can be reliably interpreted as brGDGT source shifts.

4.6. Impact of anthropogenic activities and vegetation changes on brGDGT distribution

The first decrease in ΣIIIa/ΣIIa values coincides with a shift from a thermophilous to mesophilous forest between 7.4 and 5.6 kyr cal BP (Fig. 5D). This vegetation change is also recorded elsewhere in the Massif Central (Faure, 2012; Lavrieux et al., 2013a; Cubizolle et al., 2014; Miras et al., 2015; Chassiot et al., 2018) and is thought to result from regional climatic change. Such vegetation changes progressively led to soil destabilization and thus increased terrigenous inputs into the lake of OM and magnetic minerals from the magmatic bedrock. As OM was transferred from the catchment to the lake, the proportion of soil brGDGTs increased in the lake until it dominated in situ production.

Palynological and archeological records indicate a gradual increase in human activities and their effects on erosion dynamics in the region since 6 kyr cal BP (e.g., Daugas and Raynal, 1989; Cubizolle et al., 2004; Miras et al., 2004). Pollen assemblages mark the beginning of a permanent human presence around Lake St Front from 2850 to at least 200 yr cal BP, although some phases are visible corresponding more or less with archeological periods. Each period begins with increased deforestation (a decrease of 50% of AP in 1000 years; Fig. 5D) occurring during the First Iron Age (2850–2100 yr cal BP, 900–150 BC), the Gallo-Roman period (2100–1560 yr cal BP, 150 BC–400 AD), the Middle Ages

(1560–500 yr cal BP, 390–1450 AD), and during modern times. In addition, each period is associated with increased arboriculture (*Juglans*; Fig. 5E and Supplementary Table S1), agriculture, and pastoralism in close vicinity of the lake as indicated by the increased occurrence of anthropogenic taxa such as nitrophilous taxa and cereals (e.g., *Secale*; Fig. 5E and Supplementary Table S1) whose pollen only disperse over short distances (Vuorela, 1973; Broström et al., 2008). Furthermore, at the beginning of each period, ΣIIIa/ΣIIa drops below the limit for a soil origin which points to a mostly terrigenous source for brGDGTs in sediments. The Gallo-Roman period (2100–1560 yr cal BP, 150 BC–390 AD) also shows an increase in sedimentation rate which could mark the period of greatest land use with agricultural production peaking around 1750 yr cal BP (200 AD; Fig. 5A and 5E). The increase in magnetic minerals in combination with the simultaneous decrease in OM inputs at the beginning of the Middle Ages is characteristic of exhausted agricultural soils, as continued erosion exposes the underlying magmatic bedrock. Archeological records confirm long term human occupation in the direct vicinity of Lake St Front (Dendievel, 2012 and References therein). These phases of intense land use were interspersed by brief decreases in human activity as shown by decrease in anthropogenic taxa, partial recovery of forest cover, and higher ΣIIIa/ΣIIa values.

The simultaneity of the periods of vegetation changes in the catchment area of anthropogenic or climatic origin with the changes of sedimentary fluxes and ΣIIIa/ΣIIa suggests that the changes observed in brGDGT distributions resulted from these vegetation changes. Human activities led to increased erosion by changing soil use and thus increased the quantity of OM and terrigenous brGDGTs transferred to the lake. As brGDGT distributions differ according to their origin (terrigenous vs aquatic), anthropogenic activities and climate-based vegetation changes both impact brGDGT distributions in lacustrine sediments. Changes of sedimentary fluxes thus represent a potential bias for brGDGT analysis

in lakes since they are connected with their catchment which can experience vegetation changes of anthropogenic or climatic origin. It appears necessary to understand the evolution of brGDGT sources in the past before reconstructing temperature using brGDGT distributions in lakes to detect this bias.

5. Conclusions

Characterization of brGDGT distributions in and around Lake St Front allowed the determination of their sources (terrigenous vs aquatic). Terrigenous inputs were high but significant in situ production was also detected. This indicated that brGDGTs in Lake St Front sediments have a mixed origin. Different published brGDGT source indices, weighted average number of cyclopentane moieties, degree of methyl branching of the brGDGTs and ΣIIIa/ΣIIa ratio, defined from continental and marine realms, were tested in Lake St Front sediments and nearby soils. Only the ΣIIIa/ΣIIa ratio, applied for the first time in a lake, was able to fully trace the varying abundances of terrigenous brGDGTs. The ΣIIIa/ΣIIa ratio should be tested in other lakes to determine its reliability in a variety of freshwater environments.

When applied to the sedimentary archives, a multiproxy analysis revealed that terrigenous inputs into the lake varied throughout the Holocene. A brGDGT analysis highlighted a gradual shift from aquatic to terrigenous sources with several periods of strong terrigenous inputs. These periods were synchronous with vegetation changes in the catchment area, causing soil destabilization and increased erosion. The two most recent events were associated with a continuous human occupation of the lake area from 2.8 kyr cal BP, leading to the development of agriculture, pastoralism, and deforestation. Thus, erosion dynamics that were initially driven by climatic changes were increasingly affected by human activities which became the principal forcing factor after 2.8 kyr cal BP. This demonstrated that human

activities and vegetation changes could significantly impact brGDGT distributions by modification of erosion dynamics and lead to changes in the relative proportions of terrigenous and aquatic brGDGTs.

Few paleoclimatic studies based on brGDGTs in lakes have involved identification of brGDGT sources and their potential changes over time. Studies should always control this parameter as in situ production can occur in a large range of environments including small and shallow lakes. The brGDGT source can be determined by comparing brGDGT distributions between sediments and catchment soils in the modern sets of data and by using the existing tools to determine brGDGT origin after a test in the present situation. It is also essential to associate brGDGT analysis with a multiproxy study of the evolution of the quantity of eroded soil from the catchment area delivered to the lake to identify potential external perturbations of the lacustrine ecosystem and influences on brGDGT distribution. In particular, pollen analysis can be very helpful to detect anthropogenic perturbations. These controls are necessary to prevent bias which can affect paleoclimate studies that attempt temperature reconstructions based on lacustrine archives.

Acknowledgments

We thank C. De Jonge and an anonymous reviewer for their constructive comments which improved the manuscript. We thank the CEREGE-SETEL coring team, Sébastien Marguerite and Samuel Meulé, who provided engineering and technical assistance and manpower during the coring operation with the UWITEC equipment at Lake St Front. We also thank the coring team: Guillaume Jouve, Christine Paillès, Emmanuel Chapron, Bertil Hebert and Thierry Courp. Jean Goedert is acknowledged for assisting with fieldwork during the soil sampling campaign. Sébastien Pivot and Frauke Rostek are also acknowledged for their assistance during core sampling, Guillaume Jouve for his help with core opening and

sedimentological description, and Yoann Fagault and Frauke Rostek for analytical support in the laboratory. We also thank Bassam Ghaleb for the ^{210}Pb activity measurements and advice regarding data interpretation. The ARTEMIS program and J.P. Dumoulin provided ^{14}C measurements using the Accelerator Mass Spectrometer located in Saclay, France (Laboratoire de Mesure du ^{14}C). We are also grateful to Yannick Garcin for his help with the Bacon program and to Claude Mante for his help with the compositional analysis and Codapack program. Yunping Xu is acknowledged for kindly supplying data and insightful discussions. The work at CEREGE was supported by the Collège de France. Additional financial support was provided by the BNP Paribas Foundation (Climate Initiative – project CPATEMP).

Associate Editor–**Philip Meyers**

References

Aitchison, J., 1986. The Statistical Analysis of Compositional Data. Chapman & Hall Ltd., London (UK) (Reprinted in 2003 with additional material by The Blackburn Press).

Andrieu, V., Bonifay, E., Reille, M., Rhoujjati, A., Thouveny, N., 1995. Lac de St Front. In: Quaternary Field Trips in Central Europe: International Union for Quaternary Research, XIV International Congress, pp. 1513–1518.

Ayari, A., Yang, H., Wiesenberg, G.L., Xie, S., 2013. Distribution of archaeal and bacterial tetraether membrane lipids in rhizosphere-root systems in soils and their implication for paleoclimate assessment. Geochemical Journal 47, 337–347.

Beug, H.-J., 2004. Leitfaden der Pollenbestimmung für Mitteleuropa und angrenzende Gebiete. Verlag Dr. Friedrich Pfeil, München.

Birks, H.H., Birks, H.J.B., 2006. Multi-proxy studies in palaeolimnology. Vegetation History and Archaeobotany 15, 235–251.

Birks, H.J.B., Heiri, O., Seppä, H., Bjune, A.E., 2011. Strengths and weaknesses of quantitative climate reconstructions based on late-Quaternary biological proxies. Open Ecology Journal 3, 68–110.

Blaauw, M., Christen, J.A., 2011. Flexible paleoclimate age-depth models using an autoregressive gamma process. Bayesian Analysis 6, 457–474.

Bout, P., 1973. Les volcans du Velay, itinéraires géologiques et géomorphologiques en Haute-Loire. Imprimerie Watel, Brioude.

Broström, A., Nielsen, A.B., Gaillard, M.-J., Hjelle, K., Mazier, F., Binney, H., Bunting, J., Fyfe, R., Meltsov, V., Poska, A., 2008. Pollen productivity estimates of key European plant taxa for quantitative reconstruction of past vegetation: a review. Vegetation History and Archaeobotany 17, 461–478.

Buckles, L.K., Weijers, J.W., Verschuren, D., Sinninghe Damsté, J.S., 2014a. Sources of core and intact branched tetraether membrane lipids in the lacustrine environment: Anatomy of Lake Challa and its catchment, equatorial East Africa. Geochimica et Cosmochimica Acta 140, 106–126.

Buckles, L.K., Weijers, J.W.H., Tran, X.-M., Waldron, S., Sinninghe Damsté, J.S., 2014b. Provenance of tetraether membrane lipids in a large temperate lake (Loch Lomond, UK): implications for glycerol dialkyl glycerol tetraether (GDGT)-based palaeothermometry. Biogeosciences 11, 5539–5563.

Cao, J., Rao, Z., Jia, G., Xu, Q., Chen, F., 2017. A 15ka pH record from an alpine lake in north China derived from the cyclization ratio index of aquatic brGDGTs and its paleoclimatic significance. Organic Geochemistry 109, 31–46.

Carles, J., 1956. Notice détaillée de la feuille 59 – Le Puy, de la carte de la végétation de la France au 1/200 000ème. Bulletin du Service de la Carte de la Phytogéographique. Série A, Carte de la Végétation au 200 000ème. CNRS, pp. 51–80.

Chassiot, L., Miras, Y., Chapron, E., Develle, A.-L., Arnaud, F., Motelica-Heino, M., Di Giovanni, C., 2018. A 7000-year environmental history and soil erosion record inferred from the deep sediments of Lake Pavin (Massif Central, France). Palaeogeography, Palaeoclimatology, Palaeoecology 497, 218–233.

Chen, L., Liu, J., Wang, J., Xu, G., Li, F., He, X., Zhang, Y., Li, L., 2018. Sources and distribution of tetraether lipids in sediments from the Zhejiang–Fujian coastal mud area, China, over the past 160 years: Implications for paleoclimate change. Organic Geochemistry 121, 114–125.

Colcord, D.E., Pearson, A., Brassell, S.C., 2017. Carbon isotopic composition of intact branched GDGT core lipids in Greenland lake sediments and soils. Organic Geochemistry 110, 25–32.

Comas-Cufí, M., Thió-Henestrosa, S., 2011. CoDaPack 2.0: a stand-alone, multi-platform compositional software. In: CoDaWork'11: 4th International Workshop on Compositional Data Analysis. Egozcue J.J., Tolosana-Delgado R., Ortego M.I., Sant Feliu de Guíxols.

Coûteaux, M., 1984. Bilan des recherches pollenanalytiques en Ardèche (France). Bulletin de la Société Royale de Botanique de Belgique/Bulletin van de Koninklijke Belgische Botanische Vereniging, pp. 181–196.

Cubizolle, H., Georges, V., Argant, J., 2004. Changements environnementaux et sociétés humaines dans les moyennes montagnes granitiques du Massif Central oriental au cours de l'Holocène: les enseignements tirés du croisement des données géomorphologiques, palynologiques et archéologiques. Revue d'Archéométrie 28, 57–70.

Cubizolle, H., Argant, J., Fassion, F., Latour‐Argant, C., Deng‐Amiot, Y., Dietre, B., 2014. L'histoire de la végétation depuis la fin du tardiglaciaire et l'évolution de l'emprise humaine à partir du milieu de l'holocène dans le Massif Central oriental (France).

Quaternaire. Revue de l'Association Française pour l'étude du Quaternaire, pp. 209–236.

Dang, X., Yang, H., Naafs, B.D.A., Pancost, R.D., Xie, S., 2016. Evidence of moisture control on the methylation of branched glycerol dialkyl glycerol tetraethers in semi-arid and arid soils. Geochimica et Cosmochimica Acta 189, 24–36.

Dang, X., Ding, W., Yang, H., Pancost, R.D., Naafs, B.D.A., Xue, J., Lin, X., Lu, J., Xie, S., 2018. Different temperature dependence of the bacterial brGDGT isomers in 35 Chinese lake sediments compared to that in soils. Organic Geochemistry 119, 72–79.

Das, S.K., Bendle, J., Routh, J., 2012. Evaluating branched tetraether lipid-based palaeotemperature proxies in an urban, hyper-eutrophic polluted lake in South Africa. Organic Geochemistry 53, 45–51.

Daugas, J.-P., Gilbert, A., Raynal, J.-P., 1983. Premières sépultures du Néolithique ancien en Basse-Auvergne. Bulletin de la Société d'Anthropologie du Sud-Ouest Bordeaux 18.

Daugas, J.-P., Raynal, J.-P., 1989. Quelques étapes du peuplement du Massif central français dans leur contexte paléoclimatique et paléogéographique. Variations des paléomilieux et peuplement préhistorique. Colloque du Comité français de l'Union internationale pour l'étude du Quaternaire (INQUA). Cahiers du Quaternaire n° 13. Textes réunis par Henri Laville, pp. 67–95.

Davtian, N., Bard, E., Ménot, G., Fagault, Y., 2018. The importance of mass accuracy in selected ion monitoring analysis of branched and isoprenoid tetraethers. Organic Geochemistry 118, 58–62.

De Jonge, C., Hopmans, E.C., Stadnitskaia, A., Rijpstra, W.I.C., Hofland, R., Tegelaar, E., Sinninghe Damsté, J.S., 2013. Identification of novel penta- and hexamethylated branched glycerol dialkyl glycerol tetraethers in peat using HPLC–MS^2, GC–MS and GC–SMB-MS. Organic Geochemistry 54, 78–82.

De Jonge, C., Hopmans, E.C., Zell, C.I., Kim, J.-H., Schouten, S., Sinninghe Damsté, J.S., 2014a. Occurrence and abundance of 6-methyl branched glycerol dialkyl glycerol tetraethers in soils: Implications for palaeoclimate reconstruction. Geochimica et Cosmochimica Acta 141, 97–112.

De Jonge, C., Stadnitskaia, A., Hopmans, E.C., Cherkashov, G., Fedotov, A., Sinninghe Damsté, J.S., 2014b. In situ produced branched glycerol dialkyl glycerol tetraethers in suspended particulate matter from the Yenisei River, Eastern Siberia. Geochimica et Cosmochimica Acta 125, 476–491.

Dearing, J.A., Jones, R.T., 2003. Coupling temporal and spatial dimensions of global sediment flux through lake and marine sediment records. Global and Planetary Change 39, 147–168.

Dendievel, A.-M., 2012. Définition du potentiel paléo-environnemental et géo-archéologique du Massif du Mézenc (Massif Central, France), Mémoire de Master 1 Archéo-Sciences et Géoenvironnement.

Ding, S., Schwab, V.F., Ueberschaar, N., Roth, V.-N., Lange, M., Xu, Y., Gleixner, G., Pohnert, G., 2016. Identification of novel 7-methyl and cyclopentanyl branched glycerol dialkyl glycerol tetraethers in lake sediments. Organic Geochemistry 102, 52–58.

dos Santos, R.A.L., Vane, C.H., 2016. Signatures of tetraether lipids reveal anthropogenic overprinting of natural organic matter in sediments of the Thames Estuary, UK. Organic Geochemistry 93, 68–76.

Faure, É., 2012. “Hautes terres”: l’anthropisation des monts d’Aubrac et du Lévezou (Massif Central, France) durant l’holocène : approche palynologique des dynamiques socio-environnementales en moyenne montagne. PhD Dissertation, University of Toulouse.

Fillod, A., 1985. Le Climat de la Haute-Loire. Editions de La Borne, St Vidal.

Filzmoser, P., Hron, K., 2011. Robust statistical analysis. In: Pawlowsky-Glahn, V., Buccianti, A. (Eds.), Compositional Data Analysis. Theory and Applications. John Wiley & Sons, Chichester, pp. 59–72.

Florschutz, F., 1954. Diagramme pollinique de la tourbière de Saint Front. Bulletin de la Société Académique du Puy 34, 72–73.

Gambin, B., Andrieu-Ponel, V., Médail, F., Marriner, N., Peyron, O., Montade, V., Gambin, T., Morhange, C., Belkacem, D., Djamali, M., 2016. 7300 years of vegetation history and climate for NW Malta: a Holocene perspective. Climate of the Past 12, 273–297.

Gandouin, E., Rioual, P., Pailles, C., Brooks, S.J., Ponel, P., Guiter, F., Djamali, M., Andrieu-Ponel, V., Birks, H.J.B., Leydet, M., 2016. Environmental and climate reconstruction of the late-glacial-Holocene transition from a lake sediment sequence in Aubrac, French Massif Central: Chironomid and diatom evidence. Palaeogeography, Palaeoclimatology, Palaeoecology 461, 292–309.

García-Ruiz, J.M., 2010. The effects of land uses on soil erosion in Spain: A review. CATENA 81, 1–11.

Georjon, C., Jallet, F., Lagrue, A., Loison, G., 2004. Le Néolithique ancien et moyen en Auvergne: bilan et perspectives à la lumière des données récentes. Rencontres Méridionales de Préhistoire Récente, pp. 107–132.

Ghaleb, B., 2009. Overview of the methods for the measurement and interpretation of short-lived radioisotopes and their limits. In: IOP Conference Series: Earth and Environmental Science. IOP Publishing, pp. 012007.

Günther, F., Thiele, A., Gleixner, G., Xu, B., Yao, T., Schouten, S., 2014. Distribution of bacterial and archaeal ether lipids in soils and surface sediments of Tibetan lakes: implications for GDGT-based proxies in saline high mountain lakes. Organic Geochemistry 67, 19–30.

Hammer, Ø., Harper, D.A.T., Ryan, P.D., 2001. PAST-palaeontological statistics, ver. 1.89. Palaeontologia Electronica 4, 1–9.

He, L., Zhang, C.L., Dong, H., Fang, B., Wang, G., 2012. Distribution of glycerol dialkyl glycerol tetraethers in Tibetan hot springs. Geoscience Frontiers, Geomicrobiology and Geochemistry in Extreme Environments 3, 289–300.

Hopmans, E.C., Weijers, J.W., Schefuß, E., Herfort, L., Sinninghe Damsté, J.S., Schouten, S., 2004. A novel proxy for terrestrial organic matter in sediments based on branched and isoprenoid tetraether lipids. Earth and Planetary Science Letters 224, 107–116.

Hopmans, E.C., Schouten, S., Sinninghe Damsté, J.S., 2016. The effect of improved chromatography on GDGT-based palaeoproxies. Organic Geochemistry 93, 1–6.

Hu, J., Zhou, H., Peng, P., Yang, X., Spiro, B., Jia, G., Wei, G., Ouyang, T., 2015. Reconstruction of a paleotemperature record from 0.3–3.7 ka for subtropical South China using lacustrine branched GDGTs from Huguangyan Maar. Palaeogeography, Palaeoclimatology, Palaeoecology 435, 167–176.

Huguet, A., Gocke, M., Derenne, S., Fosse, C., Wiesenberg, G.L., 2013. Root-associated branched tetraether source microorganisms may reduce estimated paleotemperatures in subsoil. Chemical Geology 356, 1–10.

Huguet, C., Hopmans, E.C., Febo-Ayala, W., Thompson, D.H., Sinninghe Damsté, J.S., Schouten, S., 2006. An improved method to determine the absolute abundance of glycerol dibiphytanyl glycerol tetraether lipids. Organic Geochemistry 37, 1036–1041.

Lambert, C., Penaud, A., Vidal, M., Klouch, K., Gregoire, G., Ehrhold, A., Eynaud, F., Schmidt, S., Ragueneau, O., Siano, R., 2018. Human-induced river runoff overlapping natural climate variability over the last 150 years: Palynological evidence (Bay of Brest, NW France). Global and Planetary Change 160, 109–122.

Lavrieux, M., Disnar, J.-R., Chapron, E., Bréheret, J.-G., Jacob, J., Miras, Y., Reyss, J.-L.,

Andrieu-Ponel, V., Arnaud, F., 2013a. 6700 yr sedimentary record of climatic and anthropogenic signals in Lake Aydat (French Massif Central). The Holocene 23, 1317–1328.

Lavrieux, M., Jacob, J., Disnar, J.-R., Bréheret, J.-G., Le Milbeau, C., Miras, Y., Andrieu-Ponel, V., 2013b. Sedimentary cannabinol tracks the history of hemp retting. Geology 41, 751–754.

Liang, J., Russell, J.M., Xie, H., Lupien, R.L., Si, G., Wang, J., Hou, J., Zhang, G., 2019. Vegetation effects on temperature calibrations of branched glycerol dialkyl glycerol tetraether (brGDGTs) in soils. Organic Geochemistry 127, 1–11.

Li, J., Pancost, R.D., Naafs, B.D.A., Yang, H., Zhao, C., Xie, S., 2016. Distribution of glycerol dialkyl glycerol tetraether (GDGT) lipids in a hypersaline lake system. Organic Geochemistry 99, 113–124.

Loomis, S.E., Russell, J.M., Sinninghe Damsté, J.S., 2011. Distributions of branched GDGTs in soils and lake sediments from western Uganda: implications for a lacustrine paleothermometer. Organic Geochemistry 42, 739–751.

Loomis, S.E., Russell, J.M., Ladd, B., Street-Perrott, F.A., Sinninghe Damsté, J.S., 2012. Calibration and application of the branched GDGT temperature proxy on East African lake sediments. Earth and Planetary Science Letters 357–358, 277–288.

Loomis, S.E., Russell, J.M., Heureux, A.M., D'Andrea, W.J., Sinninghe Damsté, J.S., 2014. Seasonal variability of branched glycerol dialkyl glycerol tetraethers (brGDGTs) in a temperate lake system. Geochimica et Cosmochimica Acta 144, 173–187.

Lotter, A.F., Birks, H.J.B., 2003. The Holocene palaeolimnology of Sägistalsee and its environmental history – a synthesis. Journal of Paleolimnology 30, 333–342.

Macaire, J.-J., Fourmont, A., Argant, J., Bréhéret, J.-G., Hinschberger, F., Trément, F., 2010. Quantitative analysis of climate versus human impact on sediment yield since the

Lateglacial: The Sarlième palaeolake catchment (France). The Holocene 20, 497–516.

Marcott, S.A., Shakun, J.D., Clark, P.U., Mix, A.C., 2013. A reconstruction of regional and global temperature for the past 11,300 years. Science 339, 1198–1201.

McKinley, J.M., Hron, K., Grunsky, E.C., Reimann, C., de Caritat, P., Filzmoser, P., van den Boogaart, K.G., Tolosana-Delgado, R., 2016. The single component geochemical map: Fact or fiction? Journal of Geochemical Exploration 162, 16–28.

Mergoil, J., 1987. Aperçu géologique du Velay. Document du CERLAT 1, 17–22.

Mergoil, J., Boivin, P., Blès, J.L., Cantagrel, J.M., Turland, M., 1993. Le Velay. Son volcanisme et les formations associées, Géologie de la France 3, 1–96.

Miallier, D., Fain, F., Sanzelle, S., 1983. Datation par thermoluminescence de tessons néolithiques d'Auvergne, in: Premières Communautés Paysannes en Méditerranée Occidentale, Colloque International UISPP. Montpellier.

Miller, D.R., Habicht, M.H., Keisling, B.A., Castañeda, I.S., Bradley, R.S., 2018. A 900-year New England temperature reconstruction from in situ seasonally produced branched glycerol dialkyl glycerol tetraethers (brGDGTs). Climate of the Past 14, 1653–1667.

Miras, Y., Vergne, V., Guenet, P., Surmely, F., 2004. Le Massif Central: premières traces d'anthropisation révélées par l'analyse pollinique des zones humides corrélées aux données archéologiques. In: Richard, H. (Ed.), Néolithisation Précoce, Premières Traces d'anthropisation du Couvert Végétal à Partir des Données Polliniques. Annales Littéraires 777, Série Environnement, Sociétés et Archéologie 7. Presses Universitaires Franc-Comtoises, Besançon, pp. 69–105.

Miras, Y., Beauger, A., Lavrieux, M., Berthon, V., Serieyssol, K., Andrieu-Ponel, V., Ledger, P.M., 2015. Tracking long-term human impacts on landscape, vegetal biodiversity and water quality in the lake Aydat catchment (Auvergne, France) using pollen, non-pollen palynomorphs and diatom assemblages. Palaeogeography, Palaeoclimatology,

Palaeoecology 424, 76–90.

Moon, J.B., Wardrop, D.H., Bruns, M.A.V., Miller, R.M., Naithani, K.J., 2016. Land-use and land-cover effects on soil microbial community abundance and composition in headwater riparian wetlands. Soil Biology and Biochemistry 97, 215–233.

Murphy, B.T., O'Reilly, S.S., Monteys, X., Reid, B.F., Szpak, M.T., McCaul, M.V., Jordan, S.F., Allen, C.C., Kelleher, B.P., 2016. The occurrence of PAHs and faecal sterols in Dublin Bay and their influence on sedimentary microbial communities. Marine Pollution Bulletin 106, 215–224.

Naeher, S., Peterse, F., Smittenberg, R.H., Niemann, H., Zigah, P.K., Schubert, C.J., 2014. Sources of glycerol dialkyl glycerol tetraethers (GDGTs) in catchment soils, water column and sediments of Lake Rotsee (Switzerland)–Implications for the application of GDGT-based proxies for lakes. Organic Geochemistry 66, 164–173.

Nakagawa, T., Brugiapaglia, E., Digerfeldt, G., Reille, M., de Beaulieu, J.-L., Yasuda, Y., 1998. Dense-media separation as a more efficient pollen extraction method for use with organic sediment/deposit samples: comparison with the conventional method. Boreas 27, 15–24.

Niemann, H., Stadnitskaia, A., Wirth, S.B., Gilli, A., Anselmetti, F.S., Sinninghe Damsté, J.S., Schouten, S., Hopmans, E.C., Lehmann, M.F., 2012. Bacterial GDGTs in Holocene sediments and catchment soils of a high Alpine lake: application of the MBT/CBT-paleothermometer. Climate of the Past 8, 889–906.

Ning, D., Zhang, E., Shulmeister, J., Chang, J., Sun, W., Ni, Z., 2019. Holocene mean annual air temperature (MAAT) reconstruction based on branched glycerol dialkyl glycerol tetraethers from Lake Ximenglongtan, southwestern China. Organic Geochemistry 133, 65–76.

Pawlowsky-Glahn, V., Buccianti, A., 2011. Compositional Data Analysis: Theory and

Applications. John Wiley & Sons, Chichester.

Pei, Q., Zhang, D.D., Li, J., Lee, H.F., 2017. Proxy-based Northern Hemisphere temperature reconstruction for the mid-to-late Holocene. Theoretical and Applied Climatology 130, 1043–1053.

Peterse, F., van der Meer, J., Schouten, S., Weijers, J.W., Fierer, N., Jackson, R.B., Kim, J.-H., Sinninghe Damsté, J.S., 2012. Revised calibration of the MBT–CBT paleotemperature proxy based on branched tetraether membrane lipids in surface soils. Geochimica et Cosmochimica Acta 96, 215–229.

Philibert, M., Dufour, D., Dufour, H., Richard, J., Richard, M., 1986. Indices d'installations d'altitude au Paléolithique moyen et au Néolithique moyen en Margeride (Massif-Central)/Traces of altitude settlements during middle paleolithic and middle neolithic in the Margeride (Massif-Central). Revue Archéologique du Centre de la France 25, 145–161.

Pouenat, P., 2007. Un tesson Villeneuve-Saint-Germain dans un lot épicardial. Archéopages pp. 74–75.

R Development Core Team, 2015. R: A language and environment for statistical computing. R Foundation for Statistical Computing, Vienna, Austria.

Reille, M., 1992. Pollen et Spores d'Europe et d'Afrique du Nord. Laboratoire de Botanique historique et de Palynologie, Marseille.

Reille, M., 1995. Pollen et spores d'Europe et d'Afrique du Nord: supplément 1. Laboratoire de Botanique Historique et Palynologie, Marseille.

Reille, M., 1998. Pollen et spores d'Europe et d'Afrique du Nord, supplément 2. Laboratoire de Botanique Historique et Palynologie, Marseille.

Reille, M., de Beaulieu, J.L., 1990. Pollen analysis of a long Upper Pleistocene continental sequence in a Velay maar (Massif Central, France). Palaeogeography,

Palaeoclimatology, Palaeoecology 80, 35–48.

Reimann, C., Filzmoser, P., Fabian, K., Hron, K., Birke, M., Demetriades, A., Dinelli, E., Ladenberger, A., 2012. The concept of compositional data analysis in practice—total major element concentrations in agricultural and grazing land soils of Europe. Science of the Total Environment 426, 196–210.

Reimer, P.J., Bard, E., Bayliss, A., Beck, J.W., Blackwell, P.G., Ramsey, C.B., Buck, C.E., Cheng, H., Edwards, R.L., Friedrich, M., 2013. IntCal13 and Marine13 radiocarbon age calibration curves 0–50,000 years cal BP. Radiocarbon 55, 1869–1887.

Rhoujjati, A., 1995. Géochimie organique et changements environnementaux du dernier cycle climatique: étude des sédiments du lac Saint Front (Massif Central, France). Aix-Marseille University.

Russell, J.M., Hopmans, E.C., Loomis, S.E., Liang, J., Sinninghe Damsté, J.S., 2018. Distributions of 5-and 6-methyl branched glycerol dialkyl glycerol tetraethers (brGDGTs) in East African lake sediment: Effects of temperature, pH, and new lacustrine paleotemperature calibrations. Organic Geochemistry 117, 56–69.

Sanchi, L., Ménot, G., Bard, E., 2013. An automated purification method for archaeal and bacterial tetraethers in soils and sediments. Organic Geochemistry 54, 83–90.

Schouten, S., Hopmans, E.C., Sinninghe Damsté, J.S., 2004. The effect of maturity and depositional redox conditions on archaeal tetraether lipid palaeothermometry. Organic Geochemistry 35, 567–571.

Shumilovskikh, L.S., Hopper, K., Djamali, M., Ponel, P., Demory, F., Rostek, F., Tachikawa, K., Bittmann, F., Golyeva, A., Guibal, F., 2016. Landscape evolution and agro-sylvo-pastoral activities on the Gorgan Plain (NE Iran) in the last 6000 years. The Holocene 26, 1676–1691.

Sinninghe Damsté, J.S., 2016. Spatial heterogeneity of sources of branched tetraethers in shelf

systems: The geochemistry of tetraethers in the Berau River delta (Kalimantan, Indonesia). Geochimica et Cosmochimica Acta 186, 13–31.

Sinninghe Damsté, J.S., Rijpstra, W.I.C., Hopmans, E.C., Weijers, J.W.H., Foesel, B.U., Overmann, J., Dedysh, S.N., 2011. 13,16-Dimethyl octacosanedioic Acid (iso-diabolic acid), a common membrane-spanning lipid of Acidobacteria subdivisions 1 and 3. Applied and Environmental Microbiology 77, 4147–4154.

Sinninghe Damsté, J.S., Rijpstra, W.I.C., Hopmans, E.C., Foesel, B.U., Wüst, P.K., Overmann, J., Tank, M., Bryant, D.A., Dunfield, P.F., Houghton, K., Stott, M.B., 2014. Ether- and ester-bound iso-diabolic acid and other lipids in members of Acidobacteria subdivision 4. Applied and Environmental Microbiology 80, 5207–5218.

Sinninghe Damsté, J.S., Rijpstra, W.I.C., Foesel, B.U., Huber, K.J., Overmann, J., Nakagawa, S., Kim, J.J., Dunfield, P.F., Dedysh, S.N., Villanueva, L., 2018. An overview of the occurrence of ether- and ester-linked iso-diabolic acid membrane lipids in microbial cultures of the Acidobacteria: Implications for brGDGT paleoproxies for temperature and pH. Organic Geochemistry 124, 63–76.

Song, M., Cheng, Z., Luo, C., Jiang, L., Zhang, D., Yin, H., Zhang, G., 2018. Rhizospheric effects on the microbial community of e-waste-contaminated soils using phospholipid fatty acid and isoprenoid glycerol dialkyl glycerol tetraether analyses. Environmental Science and Pollution Research 25, 9904–9914.

Stein, R., Littke, R., 1990. Organic-carbon-rich sediments and paleoenvironment: Results from Baffin Bay (ODP Leg 105) and the upwelling area off Northwest Africa (ODP Leg 108). In: Huc, A.Y. (Ed.), Deposition of Organic Facies. American Association of Petroleum Geologists, pp. 41–56.

Stockhausen, H., Thouveny, N., 1999. Rock-magnetic properties of Eemian maar lake

sediments from Massif Central, France: a climatic signature? Earth and Planetary Science Letters 173, 299–313.

Sun, Q., Chu, G., Liu, M., Xie, M., Li, S., Ling, Y., Wang, X., Shi, L., Jia, G., Lü, H., 2011. Distributions and temperature dependence of branched glycerol dialkyl glycerol tetraethers in recent lacustrine sediments from China and Nepal. Journal of Geophysical Research 116, G01008.

Teulade, A., Mergoil, J., Boivin, A., 1991. Etudes géologiques et volcanologiques des environs du Lac du Bouchet. In: Bonifay, E. (Ed.), Le Lac Du Bouchet (1) Environnement Naturel et Études des Sédiments du Dernier Cycle Climatique, Documents du Centre d'Étude et de Recherche sur Les Lacs, Anciens Lacs et Tourbières du Massif Central 2. Le Puy, pp. 63–78.

Tierney, J.E., Russell, J.M., 2009. Distributions of branched GDGTs in a tropical lake system: Implications for lacustrine application of the MBT/CBT paleoproxy. Organic Geochemistry 40, 1032–1036.

Tierney, J.E., Russell, J.M., Eggermont, H., Hopmans, E.C., Verschuren, D., Sinninghe Damsté, J.S., 2010. Environmental controls on branched tetraether lipid distributions in tropical East African lake sediments. Geochimica et Cosmochimica Acta 74, 4902–4918.

Tierney, J.E., Schouten, S., Pitcher, A., Hopmans, E.C., Sinninghe Damsté, J.S., 2012. Core and intact polar glycerol dialkyl glycerol tetraethers (GDGTs) in Sand Pond, Warwick, Rhode Island (USA): insights into the origin of lacustrine GDGTs. Geochimica et Cosmochimica Acta 77, 561–581.

van den Boogaart, K.G., Tolosana-Delgado, R., 2013. Analyzing Compositional Data with R. Springer, Heidelberg.

Vlag, P., Thouveny, N., Williamson, D., Rochette, P., Ben-Atig, F., 1996. Evidence for a

geomagnetic excursion recorded in the sediments of Lac St. Front, France: A link with the Laschamp excursion? Journal of Geophysical Research: Solid Earth 101, 28211–28230.

Vlag, P., Thouveny, N., Williamson, D., Andrieu, V., Icole, M., Van Velzen, A.J., 1997. The rock magnetic signal of climate change in the maar lake sequence of Lac St Front (France). Geophysical Journal International 131, 724–740.

Vuorela, I., 1973. Relative pollen rain around cultivated fields. Acta Botanica Fennica 102, 1–27.

Wang, H., Liu, W., Zhang, C.L., Wang, Z., Wang, J., Liu, Z., Dong, H., 2012. Distribution of glycerol dialkyl glycerol tetraethers in surface sediments of Lake Qinghai and surrounding soil. Organic Geochemistry 47, 78–87.

Wang, H., He, Y., Liu, W., Zhou, A., Kolpakova, M., Krivonogov, S., Liu, Z., 2019. Lake water depth controlling archaeal tetraether distributions in midlatitude Asia: Implications for paleo lake-level reconstruction. Geophysical Research Letters. doi:10.1029/2019GL082157

Weber, Y., De Jonge, C., Rijpstra, W.I.C., Hopmans, E.C., Stadnitskaia, A., Schubert, C.J., Lehmann, M.F., Sinninghe Damsté, J.S., Niemann, H., 2015. Identification and carbon isotope composition of a novel branched GDGT isomer in lake sediments: Evidence for lacustrine branched GDGT production. Geochimica et Cosmochimica Acta 154, 118–129.

Weber, Y., Sinninghe Damsté, J.S., Zopfi, J., Jonge, C.D., Gilli, A., Schubert, C.J., Lepori, F., Lehmann, M.F., Niemann, H., 2018. Redox-dependent niche differentiation provides evidence for multiple bacterial sources of glycerol tetraether lipids in lakes. Proceedings of the National Academy of Sciences 115, 10926–10931.

Weijers, J.W., Schouten, S., Hopmans, E.C., Geenevasen, J.A., David, O.R., Coleman, J.M.,

Pancost, R.D., Sinninghe Damsté, J.S., 2006. Membrane lipids of mesophilic anaerobic bacteria thriving in peats have typical archaeal traits. Environmental Microbiology 8, 648–657.

Weijers, J.W., Schouten, S., van den Donker, J.C., Hopmans, E.C., Sinninghe Damsté, J.S., 2007. Environmental controls on bacterial tetraether membrane lipid distribution in soils. Geochimica et Cosmochimica Acta 71, 703–713.

Weijers, J.W., Panoto, E., van Bleijswijk, J., Schouten, S., Rijpstra, W.I.C., Balk, M., Stams, A.J., Sinninghe Damsté, J.S., 2009. Constraints on the biological source(s) of the orphan branched tetraether membrane lipids. Geomicrobiology Journal 26, 402–414.

Weijers, J.W.H., Wiesenberg, G.L., Bol, R., Hopmans, E.C., Pancost, R.D., 2010. Carbon isotopic composition of branched tetraether membrane lipids in soils suggest a rapid turnover and a heterotrophic life style of their source organism(s). Biogeosciences 7, 2959–2973.

Weijers, J.W., Bernhardt, B., Peterse, F., Werne, J.P., Dungait, J.A., Schouten, S., Sinninghe Damsté, J.S., 2011. Absence of seasonal patterns in MBT–CBT indices in mid-latitude soils. Geochimica et Cosmochimica Acta 75, 3179–3190.

Xiao, W., Wang, Y., Zhou, S., Hu, L., Yang, H., Xu, Y., 2016. Ubiquitous production of branched glycerol dialkyl glycerol tetraethers (brGDGTs) in global marine environments: a new source indicator for brGDGTs. Biogeosciences 13, 5883–5894.

Zink, K.-G., Vandergoes, M.J., Bauersachs, T., Newnham, R.M., Rees, A.B.H., Schwark, L., 2016. A refined paleotemperature calibration for New Zealand limnic environments using differentiation of branched glycerol dialkyl glycerol tetraether (brGDGT) sources. Journal of Quaternary Science 31, 823–835.

Table 1. Sample locations, positions of stream, shoreline, and lake sediments and soil samples.

Sample name		Sample type - provenance	Latitude (°N)	Longitude (°E)	Depth (m)	Profile depth (cm)	Sampling interval (cm)
S1	a	Soil - Coniferous forest	44°58'51.05"	4°10'26.4"	0.02	2–5	Bulk
	b		44°58'47.52"	4°10'26.58"	0.02	2–5	Bulk
S2	a	Soil - Deciduous forest	44°58'51.66"	4°10'29.4"	0.02	2–5	Bulk
	b		44°58'49.02"	4°10'30.24"	0.02	2–5	Bulk
S3	a	Soil - Grassland, peaty	44°58'59.7"	4°10'21.06"	0.02	2–5	Bulk
	b		44°58'59.1"	4°10'26.4"	0.02	2–5	Bulk
S4		Soil - Peat bog	44°58'48.84"	4°9'54.72"	0.02	2–5	Bulk
S5		Soil - Grassland	44°58'47.88"	4°9'54.12"	0.02	2–5	Bulk
S6			44°58'42.96"	4°10'4.74"	0.02	2–5	Bulk
S7		Soil - Marsh	44°58'57.6"	4°10'27.72"	0.02	2–5	Bulk
R1	a	Stream sediment - Grassland/forest	44°58'46.17"	4°10'22.84"	0	0–2	Bulk
	b		44°58'46.22"	4°10'23.37"	0	0–2	Bulk
R2	a	Stream sediment - Grassland/forest	44°58'51.66"	4°10'28.5"	0	0–2	Bulk
	b		44°58'51.54"	4°10'29.1"	0	0–2	Bulk
R3	a	Stream sediment - Grassland	44°59'2.7"	4°10'21.06"	0	0–2	Bulk
	b		44°59'0.51"	4°10'2.64"	0	0–2	Bulk
R4		Stream sediment - Grassland/forest	44°59'5.16"	4°10'26.46"	0	0–2	Bulk
R5		Stream sediment - Grassland/Peat bog	44°59'3.78"	4°10'8.28"	0	0–2	Bulk
D1	a	Sediment - Shoreline	44°58'47.88"	4°9'54.12"	0	0–2	Bulk
	b		44°58'48.84"	4°9'54.72"	0	0–2	Bulk
F		Short sediment core near forest shore	44°58'53.4"	4°10'22.26"	2.5	0–25	2
P		Short sediment core near peat bog shore	44°58'57.72"	4°10'21.12"	3.2	0–30	2
O		Short sediment core near outlet	44°58'50.58"	4°9'55.8"	3.2	0–45	2
G		Short sediment core near southern grassland shore	44°58'47.34"	4°10'	2.4	0–17.5	2
SF16	1A	Short sediment core center of the lake	44°58'53.4"	4°10'14.1"	4.2	0–65	2–10
	2	Long sediment core				17–1860	10
	3					100–1300	10
SF91	B	Long sediment core	44°58'42.96"	4°10'23.4"	5.5	105–945	10
	C					900–1215	10

Table 2. ^{210}Pb measurements on bulk sediment and ages derived from the constant flux constant sedimentation model (CFCS) of the Lake St Front upper core.

Sample name	Depth (cm)	^{210}Pb dpm/g	±	CFCS age BP	±
SF16-1A-0	0.5	17.749	0.589	–64.6	0.19
SF16-1A-3	3.5	21.378	0.706	–56.5	1.30
SF16-1A-4	4.5	19.704	0.672	–53.8	1.67
SF16-1A-6	6.5	19.274	0.629	–48.4	2.42
SF16-1A-8	8.5	16.070	0.555	–43.0	3.16
SF16-1A-10	10.5	12.949	0.506	–37.6	3.91
SF16-1A-20	20.5	7.611	0.300	–10.6	7.63
SF16-1A-30	30.5	3.024	0.158	16.4	11.35

Table 3. Accelerator mass spectrometer (AMS) estimated radiocarbon ages of organic macrofossils and total organic matter from Lake St Front. Calibration was conducted using the Calib 7.10 program (Stuiver et al., 2017) and the IntCal13 curve (Reimer et al., 2013). Samples marked in bold are from Rhoujjati (1995).

Sample name	Lab. Code N° SacA	Depth (cm)	Dated material	AMS ^{14}C age BP	±	Cal year BP 1σ	Median cal year BP
SF16-coretop*	48879	1	Bulk	800	30	689–730	714
SFB2-80.2	46590	183.4	Bulk	1510	30	1347–1413	1392
SF16-3B-1-31	48889	191.8	Bulk	1885	30	1744–1880	1835
SF16-3B-1-31	48893	191.8	Plant macrofossils	1650	30	1527–1598	1553
SF16-2B-1-14	48876	194.8	Bulk	1710	30	1564–1690	1614
SF16-2B-1-55*	48892	226.8	Plant macrofossils	5920	35	6678–6783	6740
SFA-1		341	Bulk	1460	130	1281–1523	1378
SFA-2		456	Bulk	1440	120	1267–1521	1358
SF16-2C-29	48894	474.4	Plant macrofossils	1995	30	1901–1987	1945
SF16-3B-2-2	48890	488.5	Bulk	2155	30	2070–2299	2152
SFB5-49.3	46591	642.8	Bulk	3545	30	3732–3888	3839
SF16-3C-1-41.5	48895	683.6	Plant macrofossils	3730	30	3995–4146	4080
SFA-3		721	Bulk	3520	130	3638–3972	3807
SFB6-48.5	46592	747.5	Bulk	4420	30	4891–5210	5000
SFB7-6.6	46589	809.6	Sediment with macrofossils	4710	30	5328–5573	5416
SFB7-49.5	46593	852.6	Bulk	4775	30	5477–5584	5519
SFB7-71.6	46597	879.6	Plant macrofossils	4725	30	5331–5577	5471
SF16-3D-2-2.5	48891	976.5	Bulk	6285	35	7176–7254	7216
SFA-4		976.5	Bulk	5650	140	6301–6617	6455
SFB9-49	46594	1072.5	Bulk	7635	35	8393–8445	8422
SFA-5		1262	Bulk	7980	170	8592–9068	8852
SFC3-47.7	46595	1318.8	Bulk	9705	45	11,107–11,202	11,150
SF16-3E-2-30	48896	1369.5	Sediment with diatoms	10,830	70	12,687–12,767	12,729
SF16-3E-2-70	50308	1409.5	Bulk	12,620	60	14,867–15,139	14,991
SF16-3E-2-75	48878	1414.5	Bulk	12,890	70	15,256–15,527	15,396
SFC3-58.7	46596	1441.7	Bulk	13,400	60	16,029–16,228	16,124
SF16-2F-2-0.5	48880	1463.8	Bulk	15,260	90	18,421–18,638	18,528
SF16-2F-2-54.5	48881	1559.7	Bulk	19,070	130	22,752–23,149	22,964
SF16-2H-1-84.5	48882	1710.7	Bulk	25,660	290	29,463–30,259	29,854
SF16-2H-2-70.5	48883	1816.5	Bulk	29,070	420	32,751–33,731	33,169
SF16-2I-2,92.5*	48884	1993.3	Bulk	22,190	190	26,138–26,635	26,427
SF16-2J-2-44.5	48885	2162	Bulk	31,390	560	34,754–35,843	35,313
SF16-2K-1-88.5	48886	2312	Bulk	36,010	1000	39,629–41,557	40,504

SF16-2K-2-22.5*	48887	2337.5	Bulk	29,730	470	33,438–34,305	33,841

* Date rejected

Table 4. Average fractional abundances of tetra-, penta-, and hexamethylated brGDGTs and of brGDGTs with one, two, or no cycle (GDGTb, c, and a, respectively) for the catchment samples and surface sediments (0–10 cm) of Lake St Front with their isomer ratios, the summed concentrations of brGDGTs and the number of samples.

	n	Fractional abundances (%)						IR_{6Me}	IR_{7Me}	Concentration ΣbrGDGT (µg/g sed)
		%tetra	%penta	%hexa	ΣGDGTa	ΣGDGTb	ΣGDGTc			
Catchment soils and streams	18	34	48	18	88	9	3	0.19	0.02	7.09
Lake sediments (0–10 cm)	14	19	48	33	83	15	2	0.36	0.05	6.27

Table 5. BrGDGT source identification. BIT index values, weighted average numbers of cyclopentane moieties of tetra- and pentamethylated 5- and 6-Me brGDGTs, fractional abundances of tetra-, penta-, and hexamethylated brGDGTs, ΣIIIa/ΣIIa ratios, isomer ratios, and summed concentrations of brGDGTs for each surface and sub-surface sediment (0–50 cm) and catchment sample from Lake St Front.

Sample name		Depth (cm)	BIT	#rings $_{tetra}$	#rings $_{penta\ 5Me}$	#rings $_{penta\ 6Me}$	%tetra	%penta	%hexa	ΣIIIa/ΣIIa	IR_{6Me}	IR_{7Me}	Concentration ΣbrGDGT (µg/g sed)
Soils													
S1	a	2–5	0.9995	0.12	0.04	0.08	11.9	49.4	38.7	0.24	0.12	0.016	2.8
	b	2–5	0.9992	0.13	0.04	0.10	13.9	49.9	36.2	0.28	0.13	0.014	1.7
S2	a	2–5	0.9950	0.05	0.03	0.09	15.0	49.3	35.7	0.31	0.05	0.014	2.9
	b	2–5	0.9985	0.03	0.02	0.07	11.5	46.8	41.8	0.25	0.03	0.020	3.7
S3	a	2–5	0.9997	0.32	0.11	0.15	17.4	50.9	31.7	0.37	0.20	0.023	11.0
	b	2–5	0.9936	0.15	0.05	0.10	15.3	47.4	37.3	0.33	0.10	0.019	11.9
S4		2–5	0.9982	0.47	0.17	0.19	21.4	45.9	32.7	0.53	0.21	0.038	28.9
S5		2–5	0.9986	0.12	0.04	0.06	13.4	49.6	37.0	0.28	0.15	0.021	5.0
S6		2–5	0.9987	0.16	0.05	0.07	12.8	48.5	38.6	0.27	0.20	0.014	2.1
S7		2–5	0.9998	0.32	0.36	0.13	17.5	46.8	35.7	0.41	0.19	0.025	27.0
Streams													
R1	a	0–2	0.9950	0.38	0.14	0.13	21.4	48.9	29.7	0.48	0.25	0.026	5.1
	b	0–2	0.9977	0.40	0.15	0.13	23.3	48.9	27.8	0.53	0.27	0.026	10.2
R2	a	0–2	0.9970	0.27	0.09	0.09	20.6	46.1	33.3	0.47	0.23	0.021	2.7
	b	0–2	0.9983	0.29	0.09	0.09	19.5	45.8	34.7	0.46	0.22	0.019	3.8
R3	a	0–2	0.9894	0.45	0.18	0.15	25.6	46.2	28.2	0.63	0.20	0.032	2.4
	b	0–2	0.9948	0.54	0.22	0.17	25.4	46.7	27.9	0.64	0.10	0.032	7.5
R4		0–2	0.9942	0.32	0.13	0.12	21.9	46.7	31.4	0.50	0.26	0.027	0.8
R5		0–2	0.9942	0.33	0.18	0.12	15.3	50.0	34.6	0.33	0.16	0.034	1.2
Sediments													
D1	a	0–2	0.9979	0.19	0.08	0.13	28.9	48.8	22.2	0.63	0.32	0.027	1.0
	b	0–2	0.9974	0.28	0.14	0.16	28.4	49.0	22.6	0.64	0.43	0.029	1.6
F		0–1	0.9991	0.31	0.24	0.24	34.0	47.9	18.0	0.85	0.38	0.043	3.5
		2–3	0.9990	0.31	0.24	0.25	34.1	47.9	18.0	0.85	0.37	0.045	3.5
		6–7	0.9986	0.35	0.24	0.30	34.5	47.1	18.4	0.89	0.38	0.048	1.1
P		2–3	0.9990	0.33	0.28	0.25	35.2	47.1	17.7	0.92	0.35	0.055	4.8
		6–7	0.9989	0.35	0.27	0.30	36.4	46.2	17.5	0.97	0.36	0.058	1.9
O		0–1	0.9990	0.31	0.29	0.21	34.6	48.1	17.3	0.88	0.35	0.055	11.0
		6–7	0.9986	0.33	0.29	0.23	32.9	47.6	19.5	0.84	0.35	0.064	9.4
G		2–3	0.9988	0.30	0.24	0.22	32.0	48.7	19.2	0.77	0.41	0.058	3.6

	4–5	0.9988	0.31	0.25	0.20	29.1	48.9	22.0	0.70	0.36	0.074	2.9
SF16-1A	0–1	0.9986	0.33	0.31	0.23	33.6	47.6	18.8	0.87	0.33	0.062	13.9
	4–5	0.9986	0.34	0.31	0.23	33.4	47.5	19.1	0.87	0.33	0.064	15.2
	8–9	0.9983	0.34	0.31	0.23	32.9	47.7	19.4	0.84	0.33	0.066	14.2
	15–16	0.9979	0.35	0.31	0.24	33.2	47.5	19.3	0.86	0.33	0.069	14.9
	25–26	0.9976	0.34	0.29	0.25	30.8	47.8	21.4	0.79	0.32	0.070	12.0
	35–36	0.9960	0.32	0.29	0.21	29.2	47.9	22.9	0.74	0.32	0.068	10.0
	45–46	0.9943	0.32	0.30	0.17	29.5	47.8	22.7	0.74	0.32	0.066	7.4
	55–56	0.9979	0.28	0.21	0.14	24.4	46.5	29.1	0.60	0.28	0.060	9.4

Figure captions

Fig 1. Lake St Front with locations of the soil, stream, and sediment samples. A. Simplified geologic map of the Devès and Meygal-Mézenc plateaux forming the Velay region showing the location of Lake St Front with its altitude and the relevant archives at a regional scale (modified from Stockhausen and Thouveny, 1999). B. Map of Lake St Front and sampling locations for the deep sediment cores (triangles), shallow interface sediment cores (circles), soils (diamonds), streams (squares), and shoreline (crosses) along with their reference names. The catchment area is enclosed by the dotted dark red line and the woodland area is shaded in green. This topographic map was adapted from an original map provided by the Institut national de l'information géographique et forestière (IGN). C. Picture of the lake and its catchment area.

Fig 2. Age-depth model and accumulation rate for the Lake St Front sediment core.
A. Age-depth model obtained with the Bacon software (Blaauw and Christen, 2011). The grey dotted lines indicate the 95% confidence limits and the red dotted line shows the weighted mean ages for each depth. The shaded area indicates the density of individual age-depth iterations. The calibrated age range of ^{14}C-dated samples is indicated in blue. B. ^{210}Pb ages for the upper 30 cm of the core. C. Lithology of the sedimentary sequence of Lake St Front. D. Accumulation rate for the last 12,000 years cal BP obtained with the Bacon software (Blaauw and Christen, 2011). The shaded area indicates the probability density.

Fig 3. Modern brGDGT distributions. Average fractional abundance of each brGDGT in catchment soils and streams (n = 18, grey) and lake sediments (0–10 cm, n = 14, black). Average BIT index values, as well as ΣIIIa/ΣIIa and isomer ratios for each group are provided with 1σ standard deviation.

Fig 4. Compositional analysis of brGDGT distributions from catchment and sediment samples. Compositional analysis based on the fractional abundances of the 18 brGDGTs in the surface samples (IIIa″ was not considered) at Lake St Front including catchment soils and surface and sub-surface sediments (0–50 cm, n = 37). A. Scores of the brGDGT compounds on PC1 and PC2. B. Scores of the surface sediment (circles), waterlogged (filled diamonds), and other soil (open diamonds), stream (squares), and shoreline samples (crosses) along with their reference names (see Table 1). The environment of the samples has been identified as woodland (dark green), grassland (light green) or peaty (brown).

Fig 5. Sedimentological, geochemical, and palynological evolution of the Holocene recorded at Lake St Front. A. Simplified sedimentation rate obtained from the Bacon program. B. Magnetic susceptibility. C. Total Organic Carbon (TOC, Rhoujjati, 1995). D. Percentage of arboreal pollen (brown curve) and percentages of pollen from thermophilous (beige area, sum of *Acer*, *Corylus*, *Hedera*, *Ilex*, *Lonicera*, *Ostrya*, deciduous *Quercus*, *Quercus ilex* t., *Pistacia*, *Sambucus*, *Sorbus*, *Tilia*, *Ulmus*, *Viburnum*, *Viscum*) and mesophilous (green area, sum of *Abies*, *Carpinus*, *Fagus*) tree pollen. E. Cumulative percentages of pollen of nitrophilous taxa (light green area, *Plantago lanceolata*, *P. major*, *Rumex*, Chenopodiaceae, *Urtica*), cereals (orange area, Cerealia, *Secale*), and *Juglans* (burgundy area). F. C/N ratio (Rhoujjati, 1995); note that the axis has been reversed for improved readability. The dashed line represents the upper limit of production in the aquatic realm. G. BIT index with analytical errors (1σ values); note that the axis has been reversed. H. Fractional abundance of IIIa″ with analytical errors (1σ values). I. ΣIIIa/ΣIIa ratio (red curve) with analytical errors (1σ values). The dashed lines represent the upper limit of production in the terrestrial realm and the lower limit of production in the aquatic realm defined by Xiao et al. (2016). J. ^{14}C calibrated ages

and ^{210}Pb dates. Shaded rectangles highlight the periods when ΣIIIa/ΣIIa values are below the upper limit for soil origin. The period of permanent human occupation is marked by a hatched symbol. RP: Roman Period, MP: Modern Period

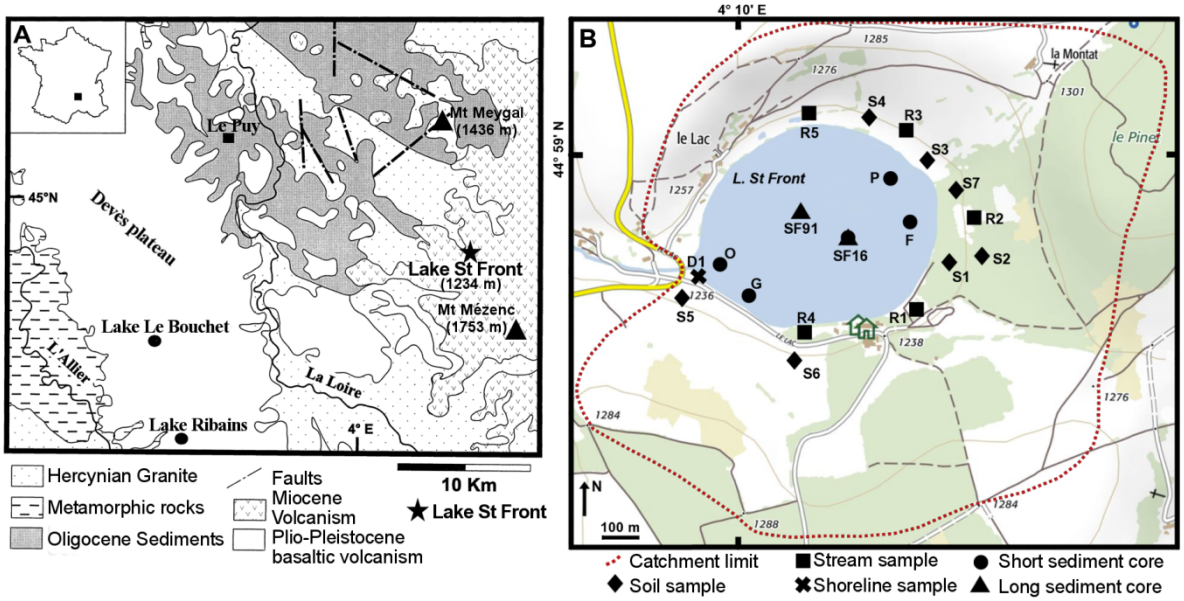

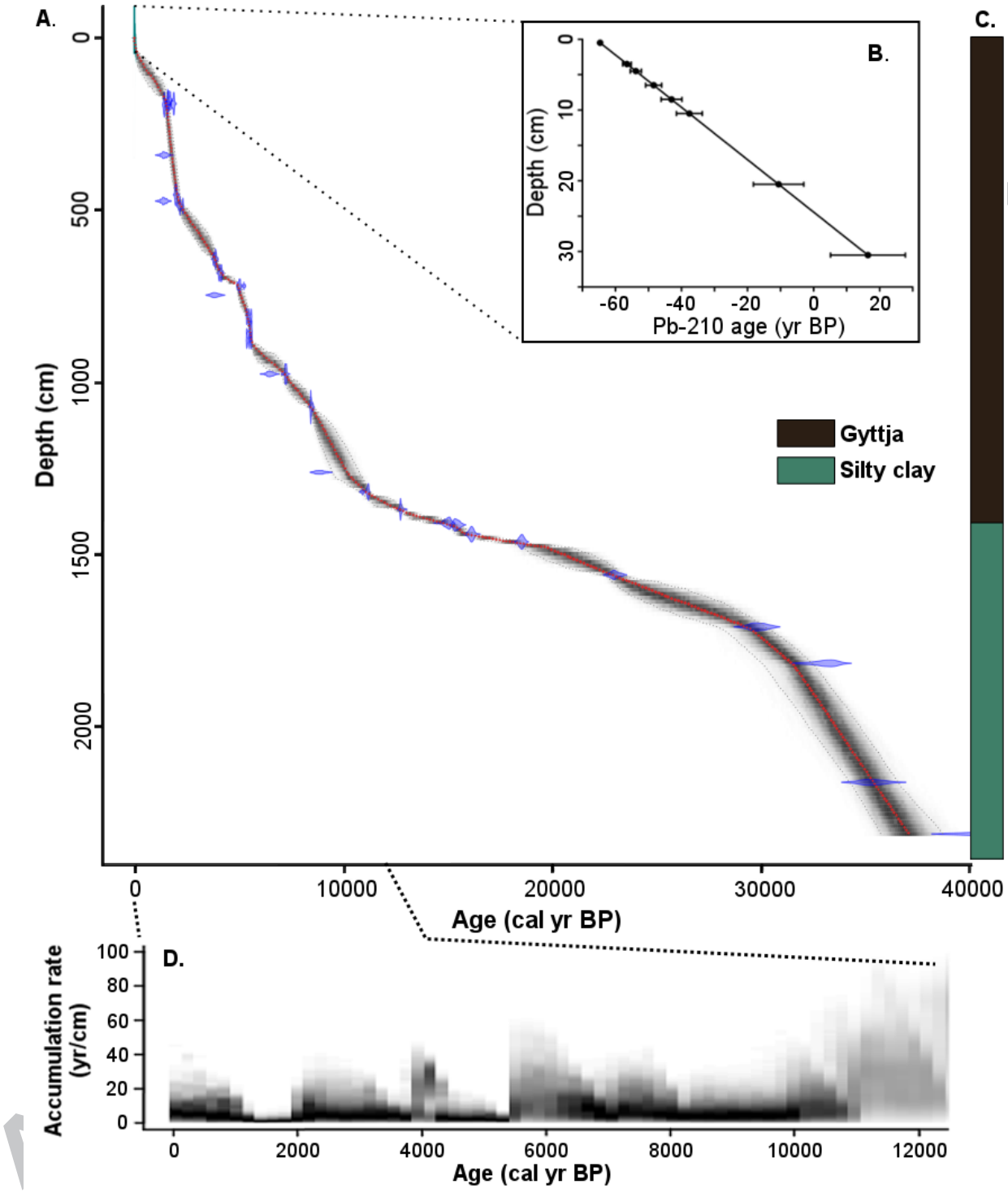
A.
B.
C.
D.
Depth (cm)
Pb-210 age (yr BP)
Gyttja
Silty clay
Age (cal yr BP)
Accumulation rate (yr/cm)
Age (cal yr BP)

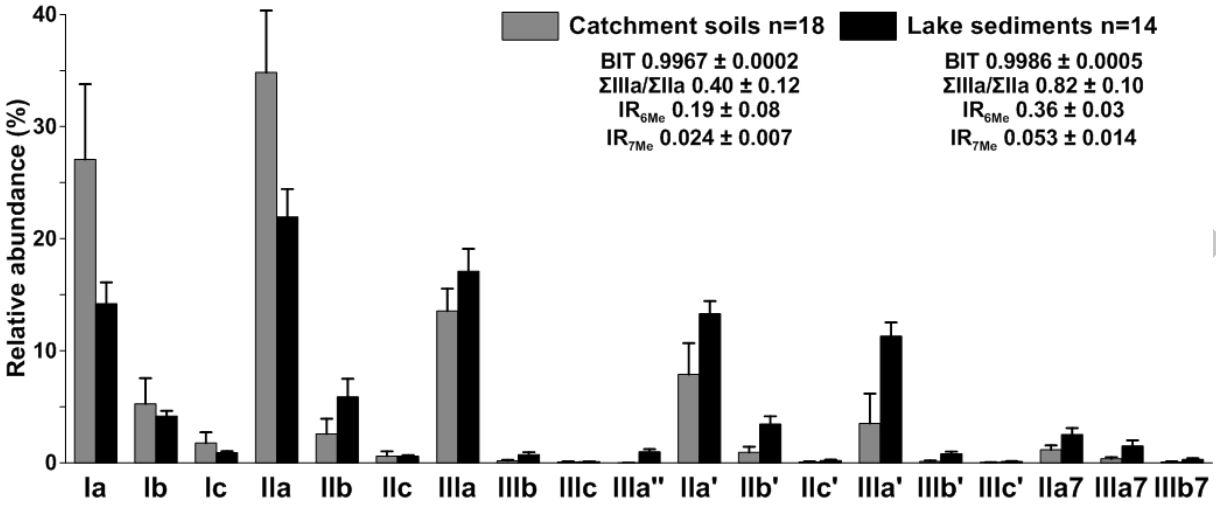
Catchment soils n=18
Lake sediments n=14
BIT 0.9967 ± 0.0002
ΣIIIa/ΣIIa 0.40 ± 0.12
IR6Me 0.19 ± 0.08
IR7Me 0.024 ± 0.007
BIT 0.9986 ± 0.0005
ΣIIIa/ΣIIa 0.82 ± 0.10
IR6Me 0.36 ± 0.03
IR7Me 0.053 ± 0.014
Relative abundance (%)
Ia Ib Ic IIa IIb IIc IIIa IIIb IIIc IIIa'' IIa' IIb' IIc' IIIa' IIIb' IIIc' IIa7 IIIa7 IIIb7

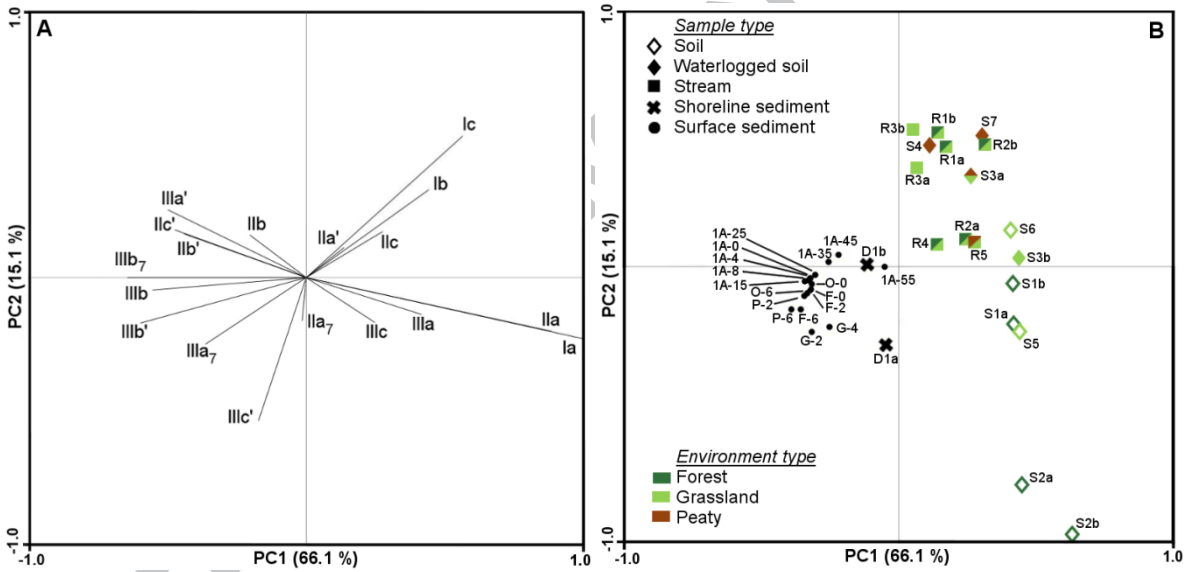
A
PC2 (15.1 %)
PC1 (66.1 %)
Ic
Ib
IIIa'
IIc'
IIb
IIa'
IIc
IIIb7
IIb'
IIIb
IIIb'
IIIa7
IIa7
IIIc
IIIa
IIa
Ia
IIIc'
B
Sample type
Soil
Waterlogged soil
Stream
Shoreline sediment
Surface sediment
Environment type
Forest
Grassland
Peaty
R3b R1b S7 S4 R2b R1a R3a S3a
R2a S6 R4 R5 S3b S1b S1a S5
1A-25 1A-0 1A-4 1A-8 1A-15 O-6 P-2 P-6 G-2 1A-45 1A-35 D1b 1A-55 O-0 F-0 F-2 F-6 G-4 D1a
S2a S2b

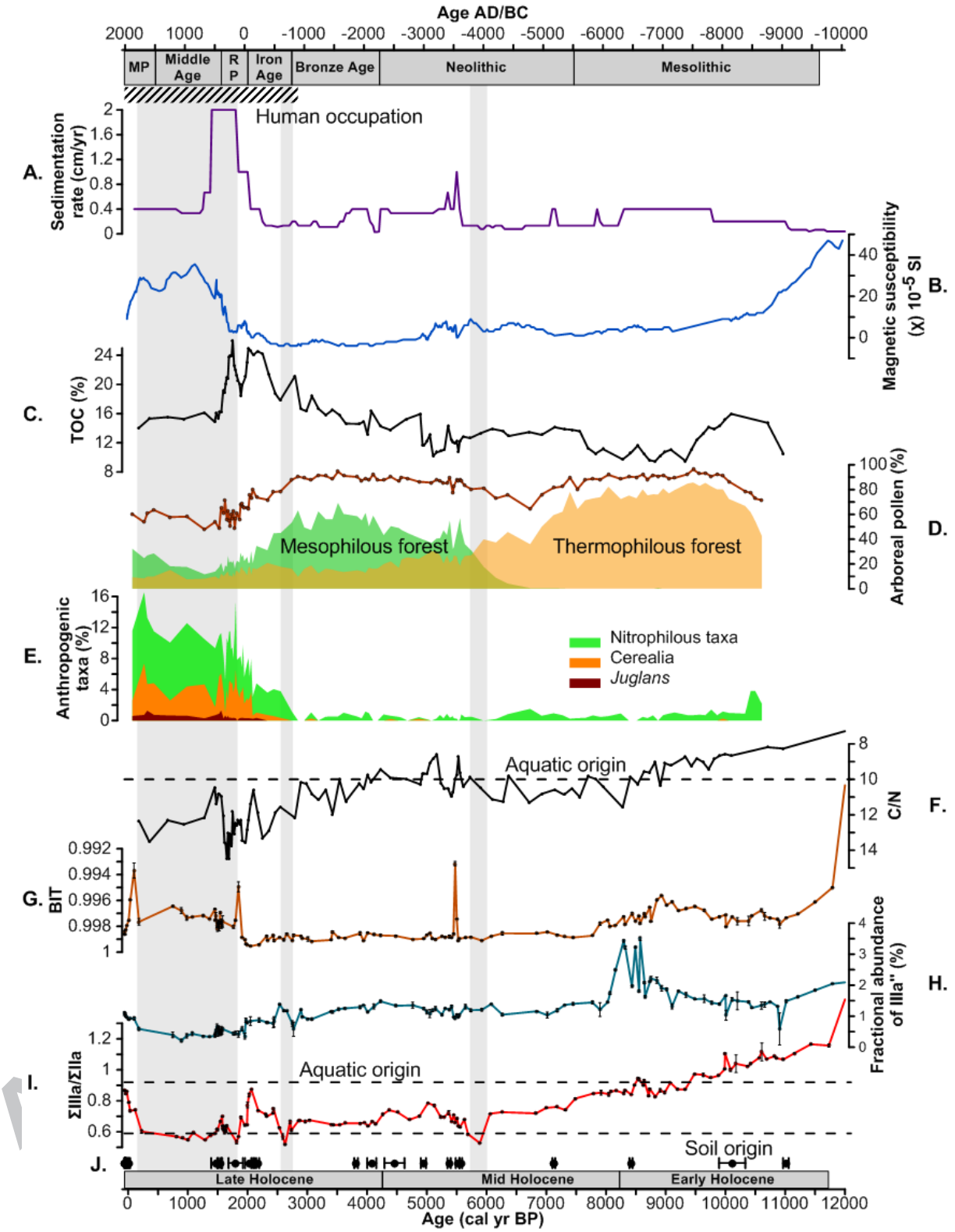

Highlights

- Downcore brGDGTs in Lake St Front sediments have a mixed origin
- ΣIIIa/ΣIIa ratio in the past can be used to reveal brGDGT source changes
- A gradual shift in brGDGT sources occurred during the Holocene in Lake St Front
- Shift in brGDGT sources results from changes in erosive dynamics of the catchment
- brGDGT distribution is impacted by vegetation changes and human activities